World Electric Vehicle Journal

MDPI

Article

Electric Vehicle Simulations Based on Kansas-Centric Conditions

Tyler Simpson, George Bousfield, Austin Wohleb and Christopher Depcik *

Department of Mechanical Engineering, University of Kansas, 3138 Learned Hall, 1530 W. 15th Street, Lawrence, KS 66045-4709, USA; tylersimpson1313@gmail.com (T.S.); george.e.bousfield@ku.edu (G.B.); amwohleb@ku.edu (A.W.)
* Correspondence: depcik@ku.edu; Tel.: +1-785-864-4151

Abstract: Range anxiety is a significant contributor to consumer reticence when purchasing electric vehicles (EVs). To alleviate this concern, new commercial EVs readily achieve over 200 miles of range, as found by the United States Environmental Protection Agency (EPA). However, this range, measured under idealized conditions, is often not encountered in real-world conditions. As a result, this effort describes the simplest model that incorporates all key factors that affect the range of an EV. Calibration of the model to EPA tests found an average deviation of 0.45 and 0.57 miles for highway and city ranges, respectively, among seven commercial EVs. Subsequent predictions found significant losses based on the impact of road grade, wind, and vehicle speed over a Kansas interstate highway. For cabin conditioning, up to 57.8% and 37.5% losses in range were found when simulating vehicles at 20 °F and 95 °F, respectively. Simulated aging of the vehicle battery pack showed range losses up to 53.1% at 100,000 miles. Model extensions to rain and snow illustrated corresponding losses based on the level of precipitation on the road. All model outcomes were translated into an Excel spreadsheet that can be used to predict the range of a generic EV over Kansas-centric roads.

Keywords: electric vehicle; modeling; range prediction; real-world; air conditioning; heating; aging

check for updates

Citation: Simpson, T.; Bousfield, G.; Wohleb, A.; Depcik, C. Electric Vehicle Simulations Based on Kansas-Centric Conditions. *World Electr. Veh. J.* **2022**, *13*, 132. https://doi.org/10.3390/wevj13080132

Academic Editors: Grzegorz Sierpiński, Roberta Di Pace and Angelo Coppola

Received: 9 June 2022
Accepted: 21 July 2022
Published: 26 July 2022

1. Introduction

While battery technology has improved significantly over the last decade, range anxiety is still a primary consideration for consumers when contemplating the purchase of an electric vehicle (EV) [1]. A recent survey by Autolist found that EV range tops consumers' list of priorities [2], with one of their earlier surveys indicating that the majority of respondents considered 300 miles of range to be sufficient [3]. While most commercially available EVs are now able to achieve greater than a 200-mile range, with the Tesla Model 3 sporting a 353-mile range according to the Environmental Protection Agency (EPA), the actual on-road range of EVs must overcome a variety of factors (e.g., weather, weight, road grade, and cabin conditioning). This distance can be significantly different than the ideal conditions employed by the EPA during the Society of Automotive Engineers (SAE) J1634 test at 77 °F using a chassis dynamometer with the cabin conditioning system turned off [4]. Driving conditions and individual drivers can also experience dissimilar ranges, with Hu et al. finding a 15.6% higher energy consumption during congested traffic conditions and up to 32.4% and 30.0% in energy consumption between drivers during peak hours and off-peak times, respectively [5]. Hao et al. similarly found that the energy consumption of EVs exceeds New European Driving Cycle (NEDC) test conditions by 7–10%, along with significant losses in winter, with EVs only achieving 64% of the expected NEDC range [6]. Thus, the varying range experienced by EV drivers can be problematic when designing a charging infrastructure to handle their range anxiety while considering the travel route and weather conditions [7]. This is especially true in Kansas when considering the wide range of conditions encountered. Kansas is the second windiest state in the union [8] and encounters all four seasons with potentially significant rainfall and snow levels [9].

Additional factors that can cause EPA vehicle range tests to misrepresent real-world driving include greater passenger and cargo loads, which will increase energy consumption [10]. Furthermore, EPA tests also do not consider road grade, which can result in increased or decreased range, depending on the slope gradient [11]. Al-Wreikat et al. found that a 3% road grade could increase energy consumption by 50% or more [12]. However, a downward grade can be beneficial, as gravity reduces the traction force needed to support a certain speed while also potentially recharging the battery pack through regenerative braking. This ability to recharge the battery pack while braking is one reason that EVs typically demonstrate a greater range in the city than on the highway, counter to more traditional internal combustion engine vehicles.

Other significant impacts on EV range are the rolling resistance and aerodynamic drag. At low speeds, when road grade is negligible, rolling resistance and drag make up the total forces acting on the vehicle that must be overcome [13]. While the EPA test does include a joint factor for both components, the impact of wind speed and direction on drag is not considered [14,15]. In addition, the increased rolling resistance due to underinflated tires can lead to EV range losses of a few percent [16]. Weather can also play a substantial role in rolling resistance, as rain can increase this resistance by up to 10% [17]. Analogously, snow can increase rolling resistance by 6–9%, depending on whether it is old or freshly fallen [18]. Thus, researchers should incorporate these effects into their models [19].

Weather further contributes to decreases in EV range when ambient temperature is considered. This is primarily due to energy being used for cabin conditioning and thermal conditioning of the battery pack. Higher temperatures typically accelerate the fading of the battery or decrease the efficiency of the motor, as Hao et al. found that electrical consumption increased by 2.3 kWh/100 km with every 5 °C over 28 °C [6]. Furthermore, Samadani et al. showed that the air conditioning system can reduce range by 14%, 20%, and 22% for the HWFET, US06, and UDDS standard drive cycles, respectively, while also increasing battery degradation [20]. Here, the impact of higher temperatures on range is not as significant as the influence of colder temperatures. Without a heater in use, the average range from different driving cycles will decrease by up to 20–30% in cold weather [18]. Conversely, when full cabin heating is in use, the range may be reduced by as much as 60% [21,22].

Apart from mechanical or electrical losses, the driving method and behavior of the driver can influence the range of an EV. Faster accelerations have been found to increase the energy intensity by 4% over the slowest acceleration simulated (1.389 m s^{-2} vs. 0.386 m s^{-2}) for a 1000 kg EV [23]. In general, aggressive driving increases energy consumption by between 16% and 43% when compared to passive driving [12,18]. This is caused by the inefficient use of the vehicle's acceleration and braking mechanisms [18].

Given this wide variance in energy usage and corresponding EV range, it is important for local municipalities and state agencies to have a simulation tool that can estimate the range of commercial EVs in their local environment. This can then be used to help the process planning of effective charging station infrastructure. While extensive models exist for motors, batteries, air conditioning, and other aspects of EVs, this effort endeavors to generate a simple overarching model that includes all necessary variables to estimate the range of EVs on local roads based on the time of year. Six commercial EVs, with their parameters provided in Table A1, were calibrated to their EPA-stated range as per the SAE J1634 test method. Parametric studies were completed to understand the various aspects that influence range over the following Kansas roads: I-70, I-35, US-54, and I-135. The interstate roads were chosen since they are the primary corridors through Kansas where EV charging stations are planned. A relatively lower-speed highway was selected for comparative purposes, and vehicle speed as a function of distance is shown in Figure 1 for one direction of these routes. In addition, the model was employed to predict the range of an EV that is not commercially available yet as an exercise to understand how the real range of the vehicle in Kansas compares to the EPA-stated range. The subsequent sections of this work include a description of the model developed, followed by a summary of the resulting parametric studies.

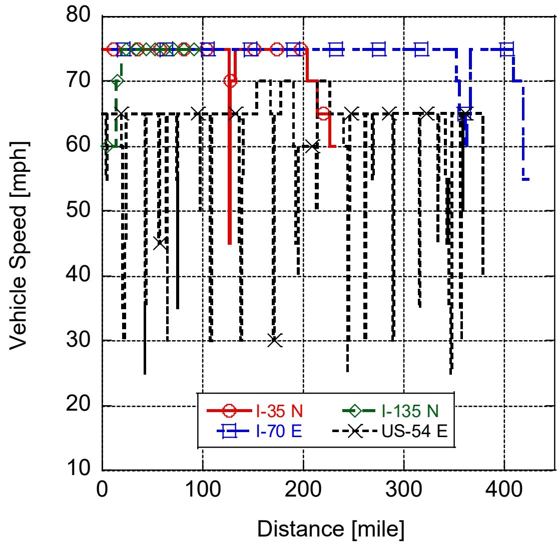

Figure 1. Vehicle speed as a function of distance for the simulated roads.

2. Modeling

A previous effort by one of the authors included the estimation of battery electric heavy-duty tractor trailers using a model based on the conservation of momentum [24]. This work used a similar model including additions to handle wind direction based on travel direction and electrical power requirements. The resultant acceleration or deceleration force (F_x) was found from the tractive (F_T), aerodynamic drag (F_D), rolling resistance (F_R), and gradation forces (F_G) as follows:

$$F_x = F_T - F_D - F_R - F_G \quad (1)$$

However, when simulating the SAE J1634 test to determine the highway and city mileage range [4], the drag and rolling resistance forces are combined and accounted for by a chassis dynamometer via a polynomial function [25] with the coefficients published online by the EPA [26]:

$$F_D + F_R = a_{EPA} + b_{EPA}\overline{V} + c_{EPA}\overline{V}^2 \quad (2)$$

where $\overline{V}$ is the average velocity of the vehicle between two successive input data points (velocity is a specified input parameter) represented by the superscript n:

$$\overline{V} = \frac{V^{n+1} + V^n}{2} \quad (3)$$

Otherwise, independent forces are seen with the drag force, indicated as:

$$F_D = \frac{1}{2}\rho A_f C_D (V_{eff} cos\varphi)^2 \quad (4)$$

where air density (ρ) is calculated from the ideal gas law, and the drag coefficient (C_D) is utilized. The vehicle's frontal area (A_f) was determined using a computer program that digitized the vehicle front view, which was calibrated to a reference value for the overall width of the vehicle [27].

2.1. Wind Speed and Direction

The actual vehicle velocity (V_{eff}) includes its yaw angle (φ) along with the speed of the wind (V_{wind}):

$$V_{eff}cos\varphi = \overline{V} - V_{wind}cos\vartheta \tag{5}$$

Yaw was assumed to be negligible since it cannot be found accurately over route length. The wind angle corresponding to the direction of motion (ϑ) included the use of latitude (*lat*) and longitude (*lon*) coordinates, which were obtained from Global Positioning System (GPS) data. The GPS data also supplied elevation (*E*) data. This choice of GPS data generalizes the model so that it can be applied for other roads through a standard method of data input.

Between two successive GPS data points, the change in distance (*d*) was calculated as:

$$d^{n+1} - d^n = R_{Earth}c \tag{6}$$

where R_{Earth} is Earth's radius (6378.1×10^3 m) [28], and *c* is determined by [29]:

$$c = 2 \times atan2\left(\sqrt{a}, \sqrt{1-a}\right) \tag{7}$$

$$a = sin^2\left(\frac{\Delta f}{2}\right) + cos(lat^n)cos\left(lat^{n+1}\right)sin^2\left(\frac{\Delta l}{2}\right) \tag{8}$$

$$\Delta f = lat^{n+1} - lat^n \tag{9}$$

$$\Delta l = lon^{n+1} - lon^n \tag{10}$$

The bearing angle of the vehicle (β_{br}) was also obtained from GPS data and altered to correspond to a 360° North (N)–South (S)/East (E)–West (W) map driving direction (q_{dr}):

$$q_{dr} = \begin{cases} 450 - \beta_{br}, & x < 0 \; and \; y > 0 \\ 90 - \beta_{br}, & else \end{cases} \tag{11}$$

$$\beta_{br} = \text{atan2}(y, x) \tag{12}$$

which outputs an angle from 0 to π or 0 to –π. Thus, q_{dr} was obtained through a piecewise function that accounts for the quadrant of the resulting vector and converts the computed angle from the "unit circle" frame to the N-S/E-W frame. The *x* and *y* components were found, respectively, as:

$$x = cos\left(lat^{n+1}\right)sin(\Delta l) \tag{13}$$

$$y = cos(lat^n)sin\left(lat^{n+1}\right) - sin(lat^n)cos\left(lat^{n+1}\right)cos(\Delta l) \tag{14}$$

The angle and speed of the wind were determined similarly from their corresponding *x*- and *y*-directions, U_w and V_w, respectively:

$$q_{wind} = \begin{cases} 450 - \text{atan2}(V_w, U_w), & U_w < 0 \; and \; V_w > 0 \\ 90 - \text{atan2}(V_w, U_w), & else \end{cases} \tag{15}$$

$$V_{wind} = \sqrt{{U_w}^2 + {V_w}^2} \tag{16}$$

This was then combined with the driving direction to find the wind angle corresponding to the direction of motion:

$$\vartheta = q_{wind} - q_{dr} \tag{17}$$

Twenty years (2000–2020) of wind speed information delineated by month for the state of Kansas was captured from National Oceanic and Atmospheric Administration data [30].

2.2. Rolling Resistance

The force due to rolling resistance in Equation (1) can be found using a single rolling resistance coefficient (μ_r) times the vehicle (m) mass and gravitational acceleration (g):

$$F_R = \mu_r m g \tag{18}$$

A more detailed option includes tire pressure (p_{tire}) and the velocity of the vehicle [31]:

$$F_R = \left(\frac{p_{tire}}{p_{ref}}\right)^{\alpha} \left(\frac{mg}{Z_{ref}}\right)^{\beta} \left(a_{rr} + b_{rr}\overline{V} + c_{rr}\overline{V}^2\right) \tag{19}$$

including reference parameters (p_{ref} = 1 kPa, Z_{ref} = 1 N). Since the model was initially calibrated to match EPA data (discussed in Section 2.7) using chassis dynamometer information (Equation (2)), this allowed for the calibration of this rolling resistance function to find the constants (a_{rr}, b_{rr}, and c_{rr}). For the parameters α and β, the values reported by Grover were utilized for a P195/70R14 tire: -0.345 and 0.929, respectively [32]. Ideally, these values should be found for each tire used by the EVs; however, this information was not available. Therefore, simulating different tire pressures and vehicle weights other than the EPA test values will incur some error. The respective trends will be informative and provide a better representation rather than the use of a singular rolling resistance coefficient. One oversight not considered with this model is that tire pressure will change based on ambient temperatures (e.g., 0.108–0.140 bar/10 °C [33]); however, this could be added in the future.

To account for inclement weather conditions, rolling resistance coefficients (μ_r) as a function of water film thickness (i.e., rain) for a standard reference test tire [34] and rolling resistance forces (F_R) based on snow thickness [35] were found, as shown in Figure 2. Using the available weights and tire pressures provided in these references, the values of the constants for Equation (19) without rain or snow were first found using the MATLAB fmincon function while minimizing the difference between the calculated μ_r or F_R based on the corresponding data:

- Rain: $a_{rr} = 9.493 \times 10^{-2}$ N, $b_{rr} = 2.111 \times 10^{-3}$ N s m^{-1}, and $c_{rr} = -5.115 \times 10^{-5}$ N s^2 m^{-2};
- Snow: $a_{rr} = -1.262 \times 10^{-1}$ N, $b_{rr} = 4.577 \times 10^{-2}$ N·s·m^{-1}, and $c_{rr} = -1.217 \times 10^{-3}$ N s^2 m^{-2}

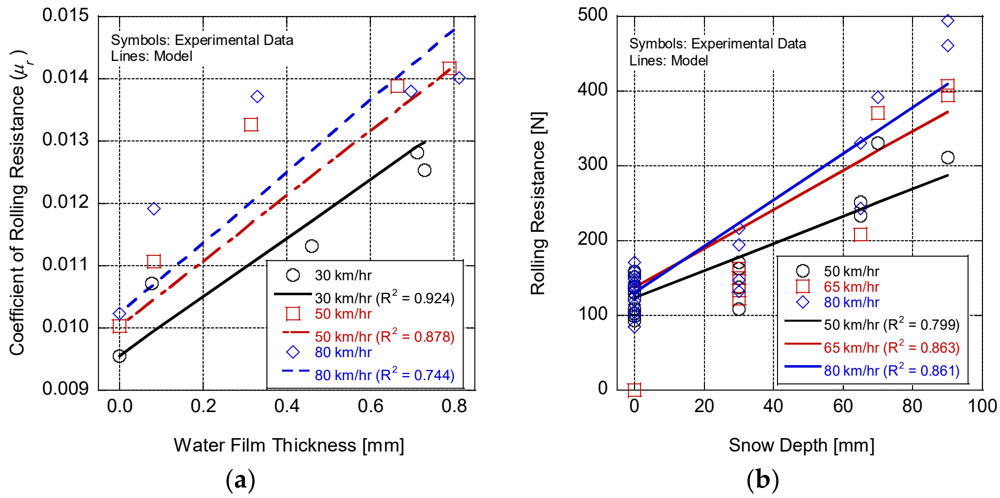

Figure 2. Comparison of rolling resistance model predictions and experimental data for (**a**) rain and (**b**) snow.

Subsequently, a revised rolling resistance force model was generated to account for the respective thickness of the rain or snow (t_{rt}), respectively:

$$F_R = \left(\frac{p_{tire}}{p_{ref}}\right)^{\alpha} \left(\frac{mg}{Z_{ref}}\right)^{\beta} \left(a_{rr} + b_{rr}\overline{V} + c_{rr}\overline{V}^2\right)\left(a_{rt} + b_{rt}t_{rt} + c_{rt}\overline{V}t_{rt}\right) \tag{20}$$

Given the respective scatter of the data, a linear fit was initially chosen, as higher-order fits caused the rolling resistance to decrease at the highest water film level, which is erroneous. Since the data also show a velocity dependency, the last term in the added model components includes its influence. This model was then calibrated using the MATLAB fmincon function to minimize the difference between the calculated values and experimental data with the following results:

- Rain: a_{rt} = 1, b_{rt} = 4.535 × 10^2 m^{-1}, c_{rt} = 4.681 s m^{-2};
- Snow: a_{rt} = 1; b_{rt} = −4.087 × 10^{-1} m^{-1}, c_{rt} = 1.081 s m^{-2}

Overall, the results in Figure 2 show an acceptable fit with R^2 values between 0.744 and 0.924. Generally, as vehicle speed increases, the rolling resistance force increases due to hysteresis losses as the tire goes through a cyclic deformation process [36]. When precipitation is present, the tire must displace the water or snow, leading to an increase in rolling resistance [37]. Thus, as shown in Figure 2, rolling resistance grows with both vehicle speed and the depth of the water or snow on the ground, as larger displacement forces are needed.

2.3. Gradation, Acceleration, and Deceleration Forces

The gradation force in Equation (1) involves the current slope of the roadway (θ):

$$F_G = mgsin\theta \tag{21}$$

which was found using the elevation change over the distance traveled:

$$\theta = \tan^{-1}\left(\frac{E^{n+1} - E^n}{d^{n+1} - d^n}\right) \tag{22}$$

Highways are required to have a maximum gradient (GP) of 7% [38]. Thus, the model limits the grade experienced to this maximum, which results in about a 4-degree slope angle:

$$\theta = \tan^{-1}(GP/100) \tag{23}$$

The net vehicle force that accounts for both deceleration and acceleration in the direction of travel equals:

$$F_x = m\frac{dV}{dt} \tag{24}$$

The derivative of velocity in this expression can be differentiated using the Euler Explicit method, thus resulting in:

$$\frac{dV}{dt} = \frac{V^{n+1} - V^n}{\Delta t} \tag{25}$$

The average vehicle speed and the distance change in travel by the vehicle are then used to find the time step in Equation (25):

$$\Delta t = \frac{d^{n+1} - d^n}{\overline{V}} \tag{26}$$

2.4. Torques, Engine Speed, and Power

At each time step, the tractive force was calculated using Equation (1), allowing for the determination of the resulting wheel (τ_w) and brake torques (τ_b), respectively:

$$\tau_w = F_T \times r_d \tag{27}$$

$$\tau_b = \frac{\tau_w}{i_0 i_g \eta_t} \tag{28}$$

where r_d, i_0, i_g, and η_t are the radius of the tire, the ratios of the final drive gear and transmission, and the efficiency of the driveline, respectively. The influence of driveline efficiency was incorporated through an auxiliary power draw, as discussed in Section 2.5; hence, for this expression, it was given a value of one.

Next, the average velocity was used to find the speed of the motor (N):

$$N = \frac{\overline{V} i_0 i_g}{2\pi r_d} \tag{29}$$

In combination with the brake torque, this value was used to determine the brake power (P_b), which was used to find the power of the motor (P_m) using the motor efficiency (η_m):

$$P_b = 2\pi \tau_b N \tag{30}$$

$$P_m = \frac{P_b}{\eta_m} \tag{31}$$

This efficiency comes from a three-dimensional map of the motor that is a function of its motor torque and speed. For simplicity, the regenerative braking map was equated to the motor map. In addition, regenerative braking power (P_r) was determined slightly differently; i.e., the power used by the motor during acceleration should be more than the braking power, whereas the power recovered by the motor during braking/regeneration should be less than the braking power:

$$P_r = \eta_m P_b \tag{32}$$

Three motor maps were found to account for two different permanent magnet synchronous motors (A-[39] and B-[40]) and an induction motor [41]), as provided in Figure 3. Unfortunately, the need to digitize these maps required estimating a few values near the origin and out of the maximum power area. In addition, if the maximum torque and maximum speed of the vehicle's motor were greater than the corresponding map chosen, then the map was scaled by these respective parameters to ensure that it captured the entire operating range. As a result, there is some error in this estimation of motor and regeneration efficiency, and it would be preferred to use the exact motor map data. Another simulation approach could be to employ the model of Larsson, which estimates motor efficiency based on torque and rotational speed, and then calibrate the constants to available map data [42]. This would provide quicker simulation results and potentially handle data near zero torque and zero motor speed more effectively.

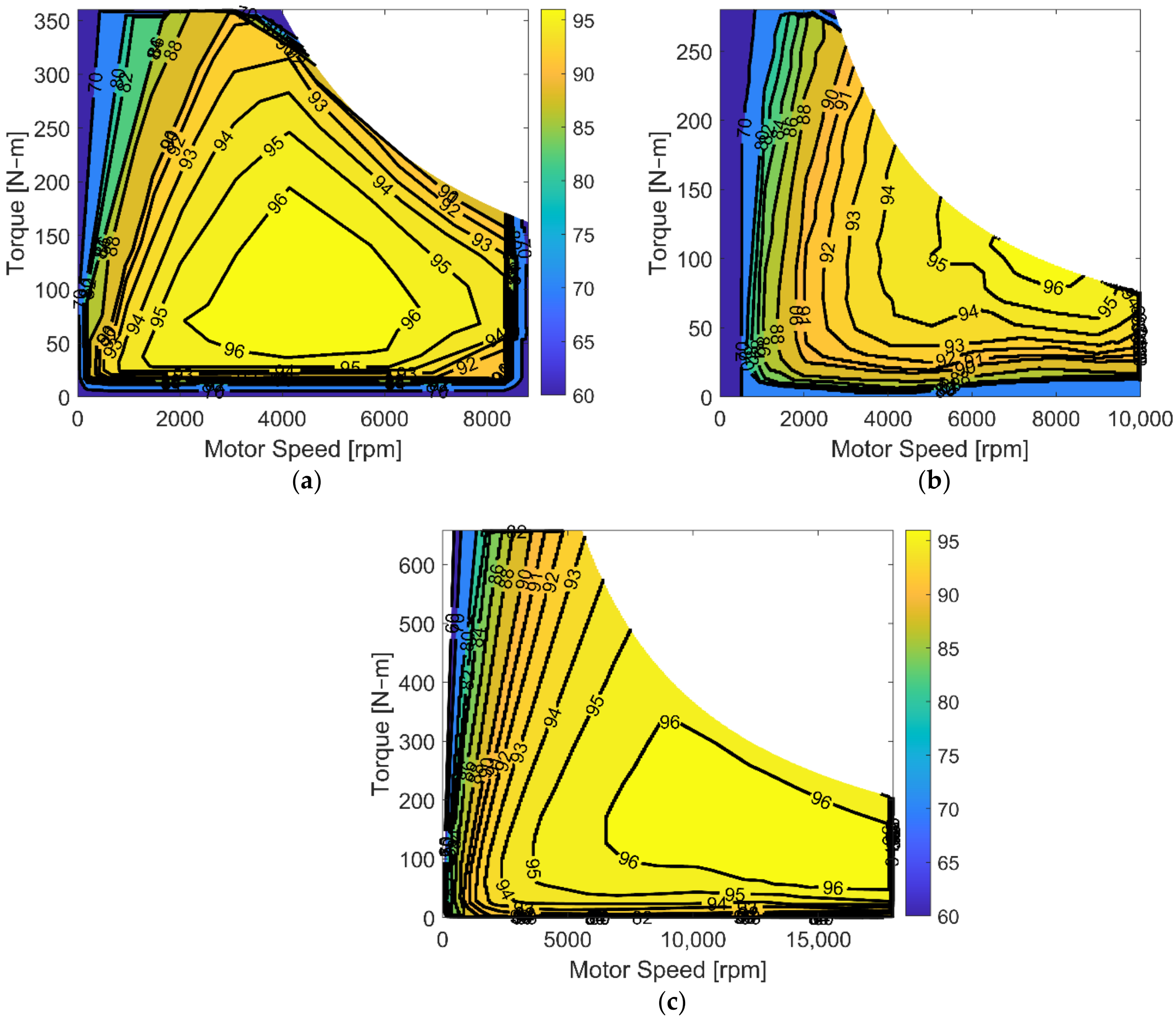

Figure 3. Digitized motor efficiency maps for (**a**) permanent magnet synchronous motor A, (**b**) permanent magnet synchronous motor B, and (**c**) induction motor. Near the origin and out of the maximum power area, a few values were estimated due to limits of the digitization process. Contour lines are indicated at 60%, 70%, 80%, 82%, 84%, 86%, 88%, 90%, 91%, 92%, 93%, 94%, 95%, and 96% efficiency values.

Subsequently, the battery pack amperage draw $\left(I_{pack}\right)$ was determined using a look-up table to determine the voltage from the current state of charge (SOC) under different discharge currents, as indicated in Section 2.6:

$$I_{pack} = \frac{P_m + P_{aux}}{\overline{V}_{pack}} \tag{33}$$

where the average voltage of the pack over the time step was used in an iterative procedure; i.e., V^n_{pack} was known, and a new value (V^{n+1}_{pack}) was found based on an updated SOC^{n+1}. The P_{aux} parameter includes all auxiliary system draws, as discussed in the next section. When the tractive force (F_T) is negative, the value of P_m is replaced by that of P_r in Equation (32), which also has a negative value. Based on its magnitude in comparison to P_{aux}, this acts to either decrease the current draw from the battery pack or add energy to the pack using the capacity model provided in Section 2.6, thus functioning as regenerative braking and extending the range of the vehicle.

2.5. Auxiliary Power

With respect to driveline efficiency, there are losses resulting from the conversion of battery energy into useful torque. Other systems, such as the inverter, lights, windows, etc., also consume energy during operation and must be considered when estimating the range of an EV. Evtimov et al. characterized these specific energy consumptions by polynomials up to the sixth order as a function of vehicle speed [43]. For the scenario in which heating or air conditioning is not needed, this power draw was estimated using a second-order polynomial while additionally including a temperature factor:

$$P_{aux,HVAC_{off}} = (a_{aux} + b_{aux}\overline{V} + c_{aux}\overline{V}^2)\left(1 + \left|\frac{T_{amb} - 298.15K}{298.15K}\right|\right)^{\alpha_{aux}} \quad (34)$$

The relatively simplistic temperature factor expression was based on findings from the American Automobile Association (AAA), which found small reductions in the driving range of commercial EVs in hot and cold ambient conditions when the heating, ventilation, or air conditioning (HVAC) system was not engaged [44]. Here, three parameters (a_{aux}, b_{aux}, and c_{aux}) were used for calibration for the model to match the SAE J1634 test for the EPA City and Highway range values (discussed in Section 2.7) at 25 °C (77 °F) with the HVAC system off [45]. The temperature factor (α_{aux}) considers the relative losses found during testing by AAA at 20 °F and 95 °F from their standard data state of 75 °F.

For the scenario in which the HVAC system is engaged, Yuksel and Michalek [46] fit the energy consumption per unit distance (E_{aux}) in [kWh mi^{-1}] to a polynomial based on the ambient temperature in [°F]:

$$E_{aux} = a_{YM} + b_{YM}T_{amb} + c_{YM}T_{amb}^2 + d_{YM}T_{amb}^3 + e_{YM}T_{amb}^4 + f_{YM}T_{amb}^5 \quad (35)$$

This model includes the effects of battery efficiency and cabin conditioning as a function of ambient conditions while isolating location-specific influences, such as driving conditions, from the effects of temperature. Similar to a prior effort [24], E_{aux} was multiplied by the velocity to obtain the power draw from the battery pack due to the HVAC system operating. However, analogous to Equation (34), a second-order polynomial was used for the velocity:

$$P_{aux,HVAC_{on}} = \left(a_{aux} + b_{aux}\overline{V} + c_{aux}\overline{V}^2\right)E_{aux} \quad (36)$$

All constants in Equations (35) and (36) were calibrated using the MATLAB *fmincon* function to minimize differences between experimental data and the model to account for the losses found from the AAA tests at 20 °F and 95 °F when the HVAC system was engaged, again away from their standard state of 75 °F. Note that temperature in Equation (35) was left in degrees Fahrenheit to be consistent with Yuksel and Michalek's formulation, and the use of kelvin provided less model fidelity; i.e., using kelvin with a sixth-order temperature term causes the value of E_{aux} to change dramatically over a 1-kelvin temperature difference.

2.6. Batteries

To calculate capacity losses or gains of the battery pack (ΔAh) as power is required or regenerated, the Hausmann and Depcik model was implemented to describe the battery capacity offset using constants γ, χ, and δ [47,48]:

$$\Delta Ah = \gamma\left(\frac{I_t}{I_{ref}}\right)^{\chi}\left(\frac{T_{ref}}{T_t}\right)^{\delta}\Delta t \quad (37)$$

The reference temperature (T_{ref}) and reference amperage draw (I_{ref}) are 298 K and 1 A, respectively. Based on the chemistry specifications of each battery for the EVs, representative singular battery voltage versus depth of discharge data were found and are provided in Figures 4–7. Unfortunately, for a few chemistries, temperature-specific data were not found; hence, the δ parameter was set to zero. Overall, data for $LiNi_{1/3}Co_{1/3}Mn_{1/3}O_2$

(NCM_{333}) [49], $LiNi_{0.5}Co_{0.2}Mn_{0.3}O_2$ (NCM_{523}) [50], $LiNi_{0.6}Co_{0.2}Mn_{0.2}O_2$ (NCM_{622}) [50], and two nickel cobalt aluminum oxide (NCA_1 and NCA_2) [51,52] batteries were found. For simulation purposes, the temperature of the battery (T_t) was set to the reference temperature since it is assumed that the battery management system endeavors to maintain the chemistry at its ideal level.

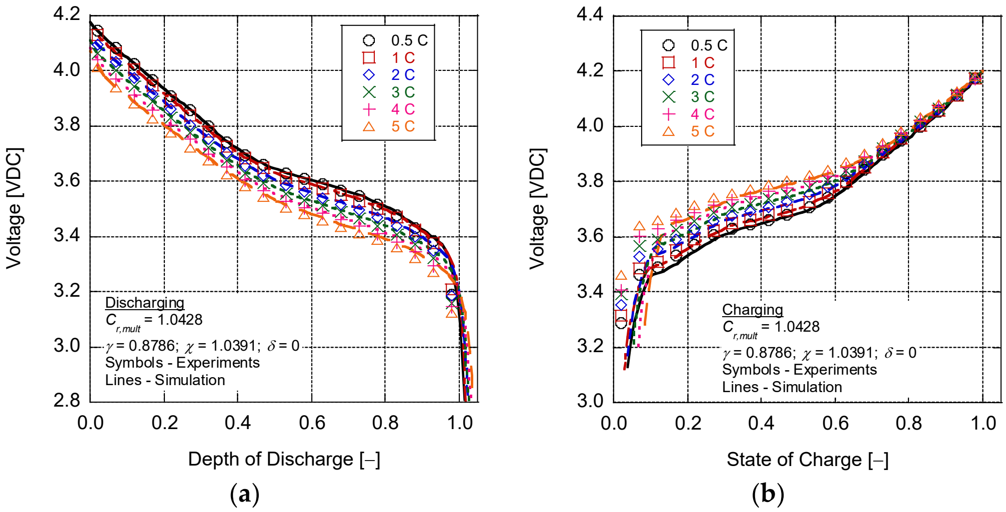

Figure 4. Experimental data and model results of a representative NCM_{622} battery during (**a**) discharging and (**b**) charging events.

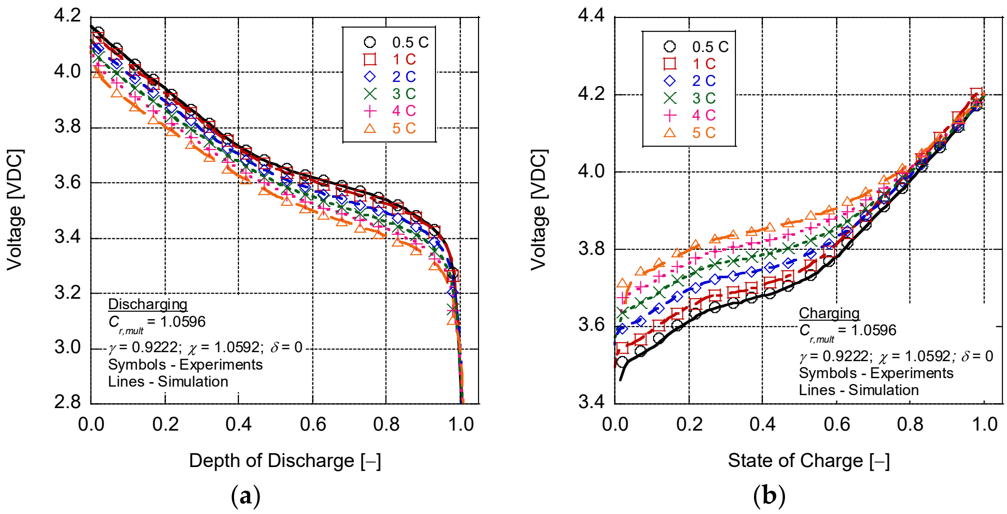

Figure 5. Experimental data and model results of a representative NCM_{523} battery during (**a**) discharging and (**b**) charging events.

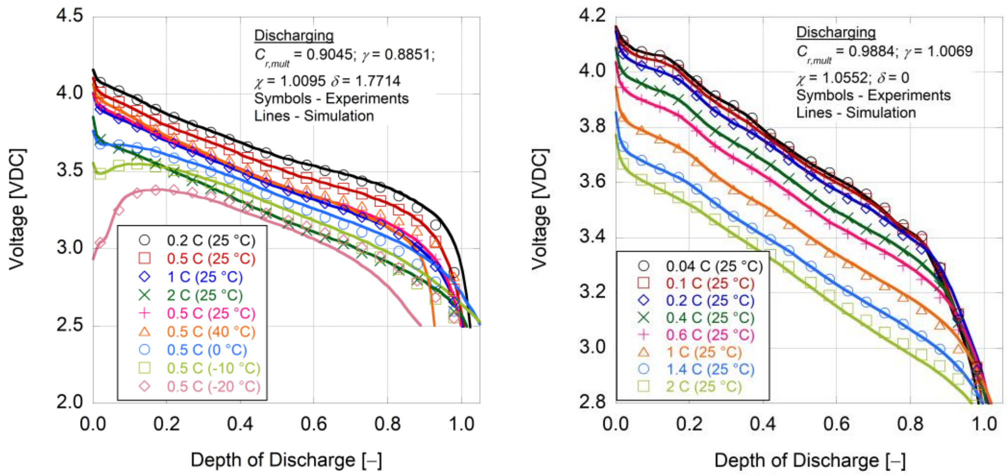

(**a**) (**b**)

Figure 6. Experimental data and model results of representative NCA batteries during discharging with (**a**) indicated as NCA_1 and (**b**) as NCA_2.

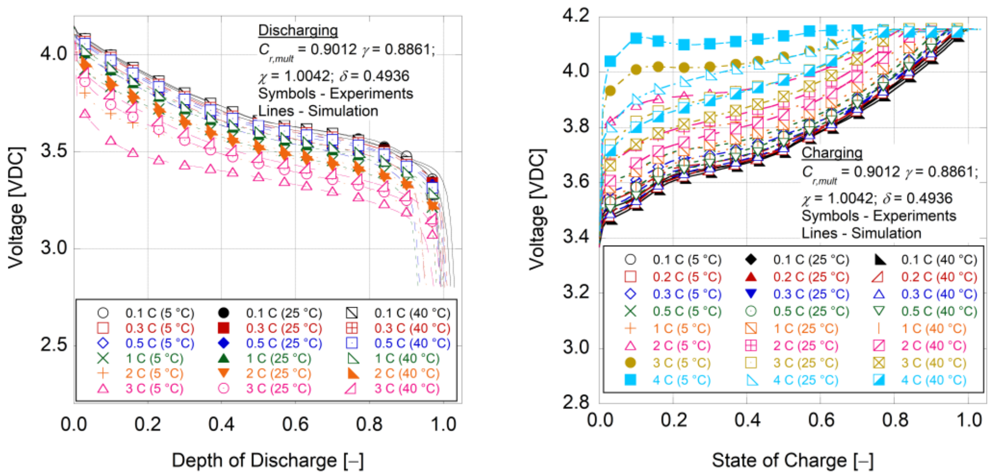

(**a**) (**b**)

Figure 7. Experimental data and model results of a representative NCM_{333} battery during (**a**) discharging and (**b**) charging events.

The calibration of the capacity offset parameters in Equation (37) follows the efforts of O'Malley et al. [48]. This model employs an absolute capacity parameter (Ah^0) that (a) replaces the arbitrariness of 20 h rate nominal capacity values, (b) includes the fact that batteries experiencing high discharge rates have remaining capacity if the discharge rate is decreased, and (c) allows for simple integration of battery aging through the degradation of the absolute capacity. The model results in Figure 4 through Figure 7 show good accuracy for all batteries, as the model is able to dynamically adjust to different currents with the absolute capacity term (equal to $C_{r,mult}$ times the nominal capacity) and parameter γ, helping to equate the energy potential to the discharge rate. The current capacity offset factor χ responds to the effective energy change and modifies the overall slope of the curve, whereas δ factors in the additional loss of capacity (or gain) as the temperature decreases (or increases). Model fidelity falters near 100% depth of discharge and at relatively low temperatures; however, these conditions should be rarely encountered by battery packs in EVs.

The simulations assume that all batteries act similarly. Therefore, the pack amperage draw was reduced by the number of batteries in parallel (N_{par}) to find the amperage required by a singular battery (I_t):

$$I_t = \frac{I_{pack}}{N_{par}} \tag{38}$$

Starting with the absolute battery pack capacity (Ah^0), the capacity of the next step (Ah^{n+1}) is determined from the capacity of the current time step (Ah^n):

$$Ah^{n+1} = Ah^n - \Delta Ah \tag{39}$$

From this information, the initial capacity is used to determine the SOC of the batteries:

$$SOC^{n+1} = \frac{Ah^{n+1}}{Ah^0} \tag{40}$$

Overall, by employing the known power draws and the simulation's time step, the energy required by the battery pack is found in watt-hours (Wh):

$$\Delta Wh = \Delta t(P_m + P_{aux}) \tag{41}$$

It has been shown that as EVs age, their range also decreases [53]. To account for this facet, polynomial curve-fits were incorporated that estimate the percentage of capacity remaining (c_m) in the battery pack after several cycles (c_y) at 25 °C:

$$\mathrm{NCM}_{622}: \ c_m = 100 - 7.525 \times 10^{-3} c_y - 1.784 \times 10^{-5} {c_y}^2 + 9.003 \times 10^{-9} {c_y}^3 - 1.507 \times 10^{-12} {c_y}^4 \tag{42}$$

$$\mathrm{NCM}_{523}: \ c_m = 100 + 7.313 \times 10^{-3} c_y - 1.764 \times 10^{-5} {c_y}^2 + 9.312 \times 10^{-9} {c_y}^3 - 1.559 \times 10^{-12} {c_y}^4 \tag{43}$$

$$\mathrm{NCA}: \ c_m = 100 - 9.312 \times 10^{-2} c_y + 7.497 \times 10^{-5} {c_y}^2 - 3.233 \times 10^{-8} {c_y}^3 + 4.745 \times 10^{-12} {c_y}^4 \tag{44}$$

$$\mathrm{NCM}_{333}: \ c_m = 100 - 3.269 \times 10^{-3} c_y - 3.223 \times 10^{-6} {c_y}^2 + 1.878 \times 10^{-9} {c_y}^3 - 3.380 \times 10^{-13} {c_y}^4 \tag{45}$$

This percentage capacity remaining was then multiplied by the initial capacity (Ah^0) to determine the pack capacity as a function of the initial starting cycle. The coefficients were determined by matching the polynomials to experimental data in Figure 8 (NCM_{622} and NCM_{523} [50], NCA [51], and NCM_{333} [49]) with an average R^2 value equal to 0.996. Note that the NCA data were linearly extrapolated from the last two data points until 3000 cycles, and the model was fit to these data for completeness.

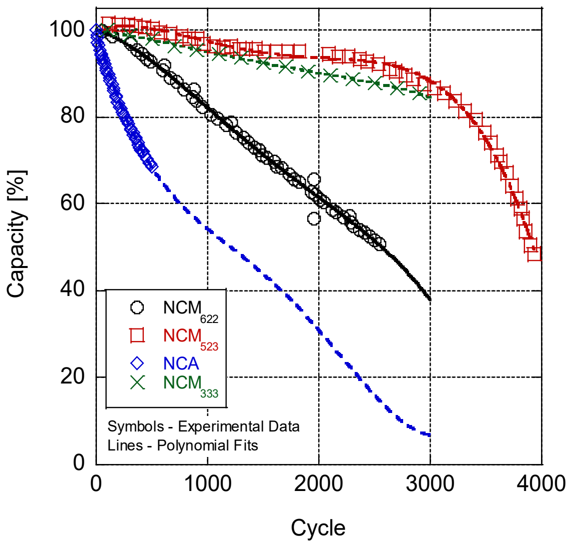

Figure 8. Loss in capacity of representative batteries based on cycle life.

2.7. SAE J1634 Calculations and Considerations

The initial calibration of the model was accomplished according to the EPA data determined from the SAE J1634 standard [4]. In this standard, the equations needed to find vehicle city and highway ranges are provided as part of a Multi-Cycle Test (MCT) procedure. The general form for the range of a given cycle type $\left(R_{cycle}\right)$ is as follows:

$$R_{cycle} = \frac{UBE}{ECdc_{cycle}} \tag{46}$$

where the total usable battery energy from the entire test (UBE) in Wh (i.e., sum of Equation (41) over the entire test) is divided by the total energy consumption per unit distance ($ECdc_{cycle}$) of a given cycle type (i.e., highway or city: Wh m^{-1}). To find $ECdc_{cycle}$, the phase scaling factor (K_{phase_i}) is used in conjunction with the energy consumption per unit distance of a given phase ($ECdc_{phase_i}$):

$$ECdc_{cycle} = \sum\left(K_{phase_i} \times ECdc_{phase_i}\right) \tag{47}$$

where $ECdc_{phase_i}$ is found using the DC energy consumption (Edc_{phase_i}) and distance traveled of a given phase (D_{phase_i}):

$$ECdc_{phase_i} = \frac{Edc_{phase_i}}{D_{phase_i}} \tag{48}$$

and K_{phase_i} is found for each phase of the test using the total number of phases of a certain cycle ($n_{UDDS} = 4,\ n_{HWFET} = 2$):

$$K_{cycle_i} = \frac{1}{n_{cycle}} \tag{49}$$

K_{phase_i} is equal to K_{cycle_i} for both phases of the HWFET (highway) cycle, but the UDDS (city) cycle requires an additional consideration. As a result of cold-start regenerative braking limitations during the first phase of the UDDS cycle that occurs during the MCT test, there is overall increased energy consumption for the UDDS cycle. To counter this effect, an equivalent phase scaling factor ($K_{UDDS_{ie}}$) is used for each UDDS phase:

$$K_{UDDS_{1e}} = \frac{Edc_{UDDS_1}}{UBE} \tag{50}$$

$$K_{UDDS_{2e}} = K_{UDDS_{3e}} = K_{UDDS_{4e}} = \frac{1 - K_{UDDS_{1e}}}{3} \tag{51}$$

Two further considerations are needed regarding the SAE J1634 standard: (1) the vehicle must be aged at least 1000 miles, and (2) the Constant Speed Cycle (CSC) at the end of the MCT must be 20% or less of the total driving distance. Regarding aging, it states that battery aging may be performed either with the vehicle [54] or by using an equivalent bench test procedure [55]. Since it was not readily apparent how to translate the bench test procedure to vehicle miles, the methodology to age the vehicle using the durability driving schedule (UDDS) was employed [54]. The UDDS cycle was simulated for 1000 miles to determine the respective number of cycles (c_y) the battery pack underwent. Then, the capacity-remaining polynomials in Section 2.6 were used to determine the respective value of c_m to be applied to the pack prior to simulating the SAE J1634 standard.

To properly model this driving cycle, values for maximum acceleration, normal acceleration, light acceleration, normal deceleration, and light deceleration had to be found from the literature. Taking the average value from various sources, 3.17 m s^{-2} and 1.01 m s^{-2} were obtained for maximum acceleration and normal acceleration, respectively [56–58]. As for light acceleration, a rate of 0.505 m s^{-2} corresponds to half of the normal acceleration value and falls within the low-to-medium range of acceleration seen in the UDDS drive cycle. For normal deceleration, an average of 2.53 m s^{-2} was found when stopping from a maximum speed ranging from 40 to 90 kph [56,59–62]. Average deceleration from maximum speeds ranging from 91 to 100 kph was significantly lower in magnitude, at an average of 1.205 m s^{-2} [62], and thus was used to model light deceleration.

As a result of these considerations, the following method was applied when calibrating the model to EPA data:

(a) Estimated a certain number of cycles based on the EPA-stated range (i.e., cycles = 1000 mi/EPA range and rounded up) to find the corresponding capacity loss from Section 2.6.
(b) Simulated the SAE J1634 test procedure and found the model parameters (e.g., auxiliary power draw and maximum *SOC*) that fit the EPA City and Highway range and miles per gallon equivalent (MPG_e) while ensuring that the 20% or less requirement for the CSC at the end (CSC_{end}) was met (note: additional code was generated to dynamically create the MCT profile as indicated in Figure 9).
(c) Using the EPA combined drag and rolling resistance model in Equation (2) from 0 to 100 miles per hour while calculating the individual drag force via Equation (4), the rolling resistance coefficients (a_{rr}, b_{rr}, and c_{rr}) in Equation (19) are calibrated. Like other calibration efforts, the MATLAB fmincon optimization routine was utilized to minimize the difference between the two models.
(d) Ran with the calibrated rolling resistance and drag information through the durability driving cycle routine over 1000 simulated miles to see if it altered the number of cycles from (a).
(e) If it did change, (b) was performed again using the new number of cycles, and the procedure was repeated.

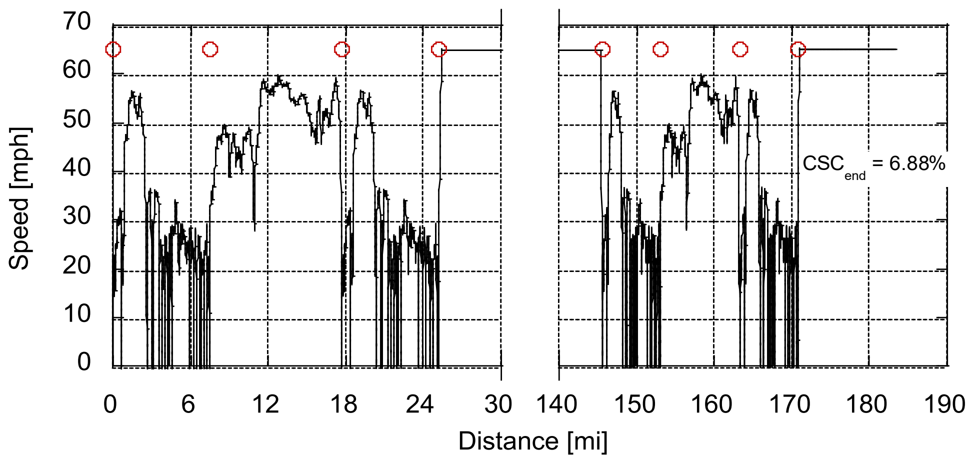

Figure 9. Created MCT cycle for the 2019 Chevy Bolt. The red circles correspond to the beginning and ending of the different components of the cycle (UDDS, HWFET, and CSC).

At this point, the model was fully calibrated to the SAE J1634 test procedure.

3. Results

In Table A1, all EV specifications and model parameters that were found (or estimated) are provided. In the following sections, the results of the model are described according to the influence of different parameters that affect their range.

3.1. SAE J1634 Results including Vehicle Mass and Tire Pressure

Since the authors are not privy to the exact specifications of each vehicle and drivetrain, when trying to match the EPA-stated ranges, it was decided to let the maximum *SOC* of the battery pack be a calibration parameter. Investigating the representative batteries in Figure 4 through Figure 7, it was assumed that most EVs would not want to operate at a greater than 90% depth of discharge (10% *SOC*) since the voltage falls dramatically and the battery's chemistry can be damaged. For similar reasons, operating at greater than 80% *SOC* might not be preferred, with Kostopoulos et al. finding that most researchers suggest a 20–80% *SOC* range for reduced capacity degradation while maintaining a good cyclical performance [63]. This assumption worked relatively well, with five of the vehicles demonstrating an *SOC* range from 0.1 to ~0.85. For the VW e-Golf, the *SOC* range had to be expanded to nearly the maximum to match EPA data. While this outcome is not realistic, concessions must be made when not all information is readily available. Overall, on average, the model deviates from the EPA highway and city range by 0.45 and 0.57 miles, respectively, for the six simulated vehicles listed in Table A1.

Figure 10 illustrates the influence of increased vehicle mass and tire pressure during a representative EPA test of the Chevy Bolt. As expected, adding vehicle mass reduces the range of the vehicle with around a 1–2% loss in range after doubling the added vehicle mass (300 lbs is added as required in the SAE J1634 test procedure). Similarly, reducing the tire pressure shows a small corresponding loss in range of around 1% when the tire pressure is decreased by 2 psi. As stated previously, the EPA test procedure is accomplished using a chassis dynamometer and does not include the influence of wind or road grade. In addition, it is carried out without employing an HVAC system or even operating at most highway speed limits (i.e., its maximum speed is 65 mph, as indicated in Figure 9); thus, it does not generally stress the battery pack. The relatively small losses according to added vehicle mass and tire pressure indicated in Figure 10 are likely underpredicting what would be experienced in a real-world scenario.

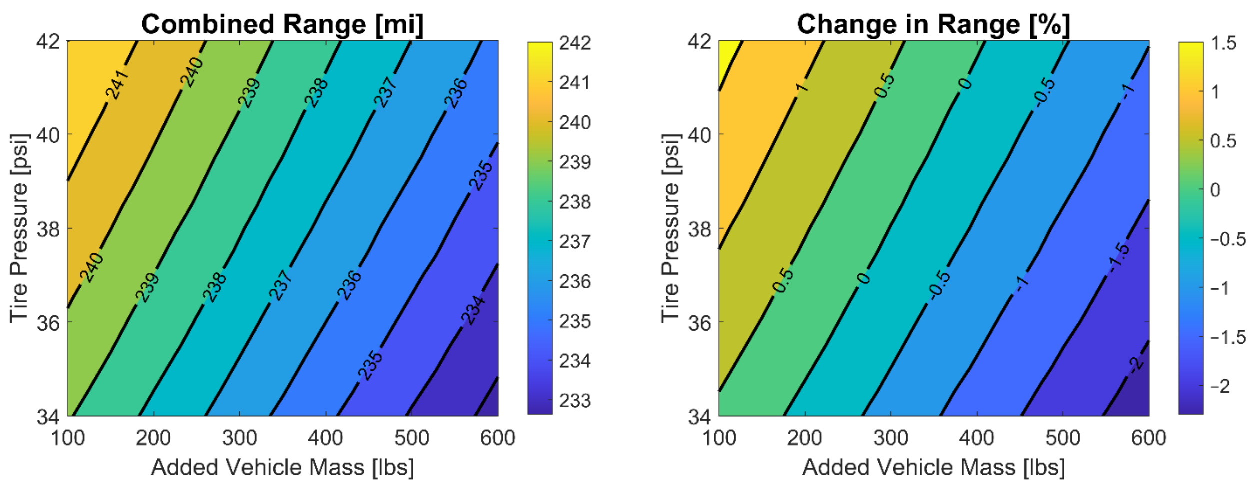

(**a**) (**b**)

Figure 10. (**a**) Combined range in miles and (**b**) percentage change in range for a Chevy Bolt based on the added vehicle mass and tire pressure.

3.2. Road Grade, Wind, and Vehicle Speed

As a test of real-world conditions, the Nissan Leaf model was simulated driving from Kansas City, MO, USA (222.77 m elevation), to the Colorado border (1172.80 m elevation) along I-70 West at EPA test ambient conditions. Since the EPA test is performed at a maximum speed of 65 mph, immediately upon simulation of true highway speeds (note: GPS location data were correlated to the posted speed limit), a Nissan Leaf loses 36.2% of its range without considering road grade and wind conditions, as indicated in Figure 11. Subsequently, since traveling to the Colorado border has a relatively uphill grade, the vehicle now loses 37.2% of its EPA-stated range when considering road elevation. In addition, in most months, traveling West on I-70 meets a wind force counter to vehicle motion; thus, adding the negative impact of wind from June 2020 shows a 40.1% total range decrease. Finally, since a significant majority of drivers often drive faster than the posted speed limit [64–66], increasing the maximum speed of the vehicle to 80 mph (in the posted

75 mph speed limit zones) while factoring in wind and road grade demonstrates an overall 43.2% loss in the EPA-stated range.

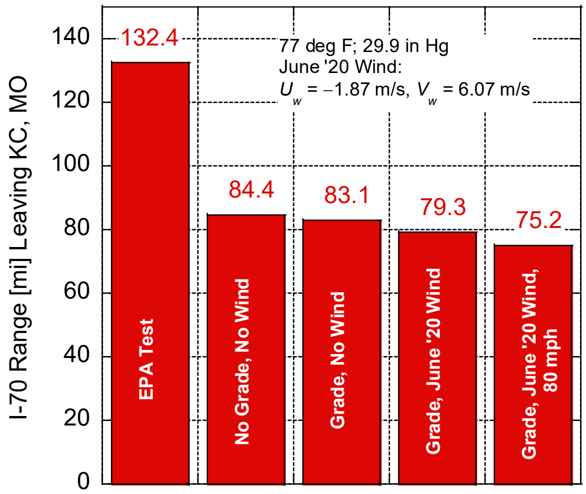

Figure 11. Illustration of road grade, wind, and vehicle speed influences on range of Nissan Leaf under EPA-tested ambient conditions.

3.3. Ambient Temperature Conditions

To account for just the effect of different ambient temperatures, as discussed in Section 2.5, the α_{aux} parameter of Equation (34) was calibrated to the AAA data, which led to reductions in driving range with the HVAC system off. Of note, AAA performed their tests according to the SAE J1634 method while including an additional driving cycle. This effort ignored the influence of this additional driving cycle and simply used the respective losses in city and highway mileage as a function of the two temperatures tested (20 °F and 95 °F) from AAA's base temperature data (75 °F). This was applied for all vehicles where AAA data existed, and the other vehicles used an average value of α_{aux}. Overall, the model deviated from the experimental data by 1.90/3.53 and 4.78/3.03 miles for the city and highway ranges at 20 °F and 95 °F, respectively. Obviously, the losses due to ambient temperature conditions are more complex than what a single parameter can estimate; however, without more information about the vehicles, this simplistic model provides a reasonable result.

Continuing the examination of the Nissan Leaf from the prior section, the respective range of this vehicle over the I-70 highway heading West was explored at the posted speed limits based on the ambient temperature. In Figure 12, the range of the vehicle is indicated before recharging is required when the HVAC system is not engaged; thus, each "leg" of the journey is provided based on the month of travel. Interestingly, a wide variance is seen as the wind direction changes from helping (December to February) to hurting (March to November). Overall, it would take five recharging stops to reach the Colorado border and six when the wind direction is negatively influencing drag on the vehicle. In comparison, the EPA-stated highway range predicts that only three recharging events would be needed; thus, up to 2 × the number of charging events might be encountered by the driver.

To account for the influence of the engaged HVAC system, the AAA data including the added effect of HVAC was utilized to determine the power draw parameters of Equations (35) and (36). Similarly, model calibration using the MATLAB fmincon function utilized the respective losses in city and highway mileage as a function of the two temperatures tested from their base temperature data. On average, at 20 °F, the model deviates by 8.68 and 7.35 miles for the city and highway ranges, respectively, whereas, at 95 °F, the model deviates by 2.83 and 2.90 miles, respectively, for the city and highway predictions. Ideally, more data points beyond two temperatures should be used to help calibrate the model or fabricate a better model. However, the present model should still generate a relatively more realistic outcome under real-world conditions than the SAE J1634 test procedure.

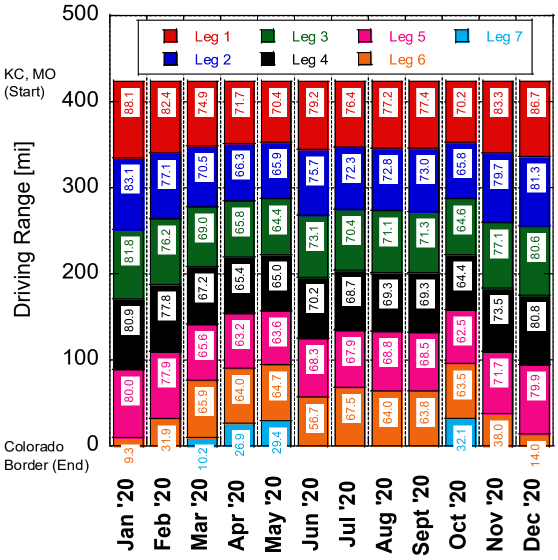

Figure 12. Traveling from Kansas City, MO, to the Colorado border on I-70 West with the respective range shown before charging is necessary. HVAC system is not engaged.

Figure 13 shows the influence of engaging the HVAC system of the same vehicle (Nissan Leaf), but now driving from the Colorado border to Kansas City, MO, on I-70 East. Interestingly, using the January 2020 data shows that the vehicle now needs seven recharging events when the HVAC system is engaged. For this month, the relatively wintry weather increases the requirements of the heating system, with the greater density of air and the negative impact of wind now increasing vehicle drag. On average, for each leg that used the full *SOC* of the battery pack, turning on the HVAC system lost around an additional 4.4 miles of range over the entire year. Compared to the EPA-stated range of 132.4 miles, complete legs heading East on I-70, with its beneficial road grade, had an average range of 75.1 miles (43.3% less) over the course of the year.

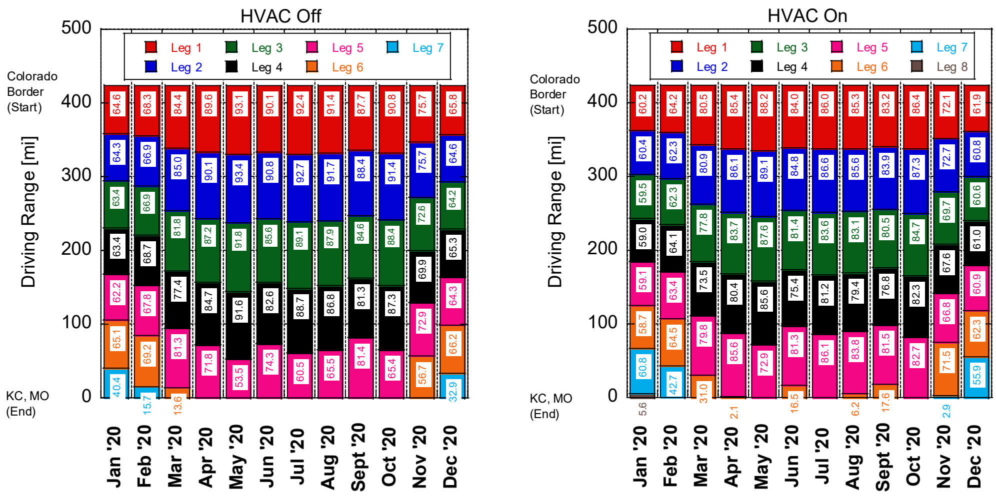

(**a**) (**b**)

Figure 13. Traveling from the Colorado border to Kansas City, MO, on I-70 East with the (**a**) HVAC system off and (**b**) HVAC system on for the Nissan Leaf.

Figure 14 provides the modeled range of the vehicles for the SAE J1634 test procedure simulated as a function of ambient temperature with the engagement of the HVAC system.

Given the sparseness of data used for calibration, caution should be employed when using these models; however, the overall trend of range with ambient temperature follows the respective trend predicted by EV data [67]. The Tesla Model 3 and Jaguar I-Pace HVAC models were generated by scaling the respective average P_{aux} in Equation (36) using the vehicle cabin sizes (V_{cabin}) between the corresponding resistance heating (Chevy Bolt and Tesla Model S) and heat pump (Nissan Leaf and VW e-Golf) vehicles:

$$P_{aux,Model\ 3} = F{\cdot}average\left(\frac{P_{aux,Bolt}}{V_{cabin,Bolt}}, \frac{P_{aux,Model\ S}}{V_{cabin,Model\ S}}\right)V_{Cabin,Model\ 3} \quad (52)$$

while additionally finding a factor (F) that ensures the HVAC-on model predicts at least 5% lower city and highway range than the corresponding HVAC-off model for that vehicle at each temperature. The values in Table A1 are the resulting parameters from these estimations.

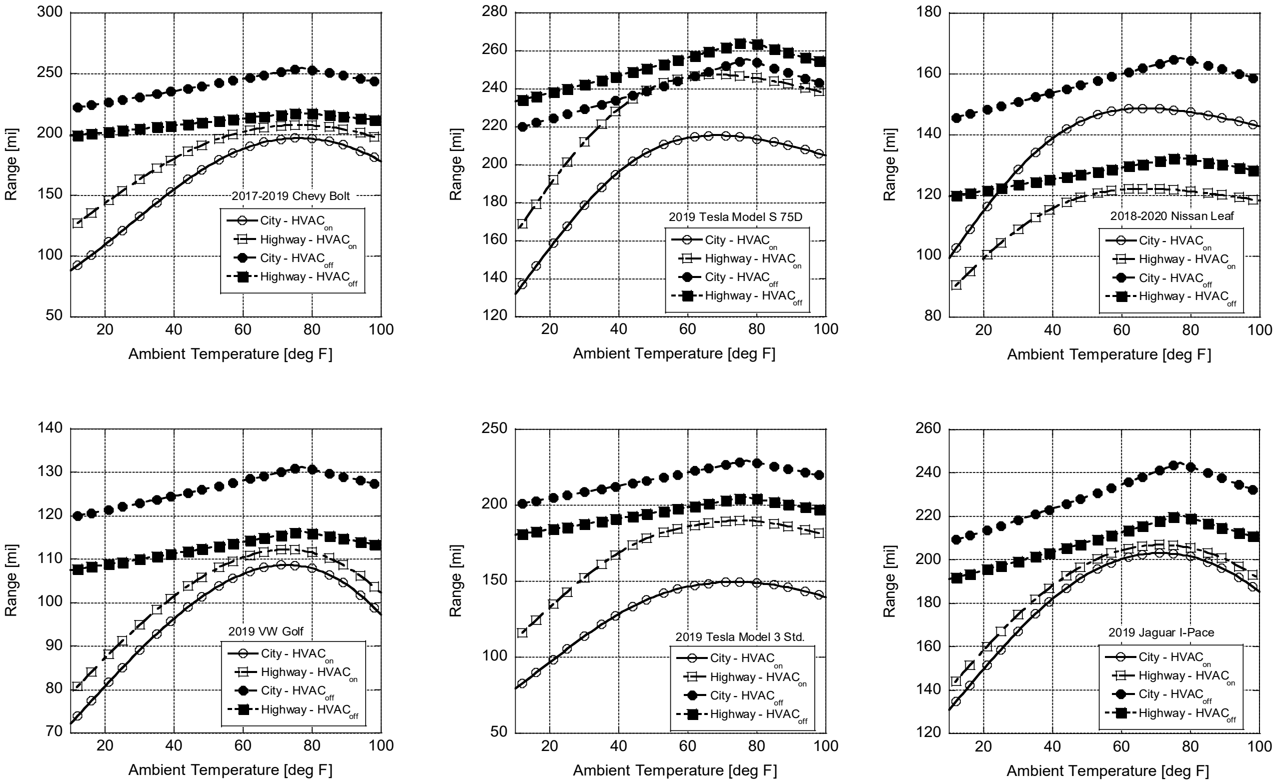

Figure 14. Range of the different modeled vehicles based on ambient temperature with the HVAC system off (solid symbols) and HVAC system on (open symbols) for the SAE J1634 test procedure.

As shown, the vehicles that employ a heat pump lose less range as a function of ambient temperature than the vehicles using resistance heaters. This is to be expected given the relative inefficiency of resistance heaters with heat pumps for EVs, showing Coefficients of Performance of around 2 [68]. Thus, more companies are investigating the potential of heat pumps while factoring in the additional cost required for this technology [69]. Based on the Nissan Leaf and VW e-Golf losses, the use of scaling via Equation (52) first appears to overpredict the range loss for the Jaguar I-Pace. However, given the lower EPA range of these vehicles in comparison to the I-Pace, when normalized, the percentage loss is relatively consistent: at 20 °F. The Leaf and e-Golf lose 30.4% and 38.5% of their range, whereas the I-Pace is predicted to lose 38.8% of its range. Interestingly, Christen et al. found that battery electric vehicles lose about 30–50% of their range at 20 °F and around 20% of their range at 95 °F [69]. The model predictions here indicate losses (city or highway) from

24.9–57.8% at 20 °F to 8.1–37.5% at 95 °F; thus, it appears that the models generated here provide reasonable values.

3.4. Vehicle Aging

As EVs age and the number of battery cycles undergone increases, Figure 8 demonstrates that the overall capacity of the battery pack will decrease. This could exacerbate the range anxiety of the consumer and possibly lead to the consumer returning to a petroleum-based vehicle. Interestingly, the accuracy of the predicted range of the vehicle was shown to account for around 20% of the satisfaction of an EV owner [70]. Thus, it is important to understand how the range of an EV will change based on the driving location and the vehicle mileage.

Figure 15a shows the range of the Jaguar I-Pace driving North on I-35 at various times in the year 2020 as the vehicle ages. The age of the vehicle was estimated by taking odometer mileage and dividing by the EPA-stated combined range to determine the cycle to use with the models developed for Figure 8. This is an underestimation of the number of cycles but should provide sufficient insight. Again, each month shows a different range of the EV, with the respective temperature and wind direction playing a role. Since the Jaguar was simulated using the NCM_{622} battery, which has a relatively linear decrease in capacity with cycle usage, the range generally drops linearly with odometer mileage (shown here on a logarithmic x-axis). At around 90,000 miles, the vehicle has lost 5% of its range for that month, and with subsequent driving, the loss continues up to around 15% at 200,000 miles. At 100,000 miles, the Jaguar averages 124.4 miles of range over the year, a 43.7% decrease from its EPA-estimated 220.8 highway mile range, but only a 5.7% loss in range from its predicted range at 1000 miles.

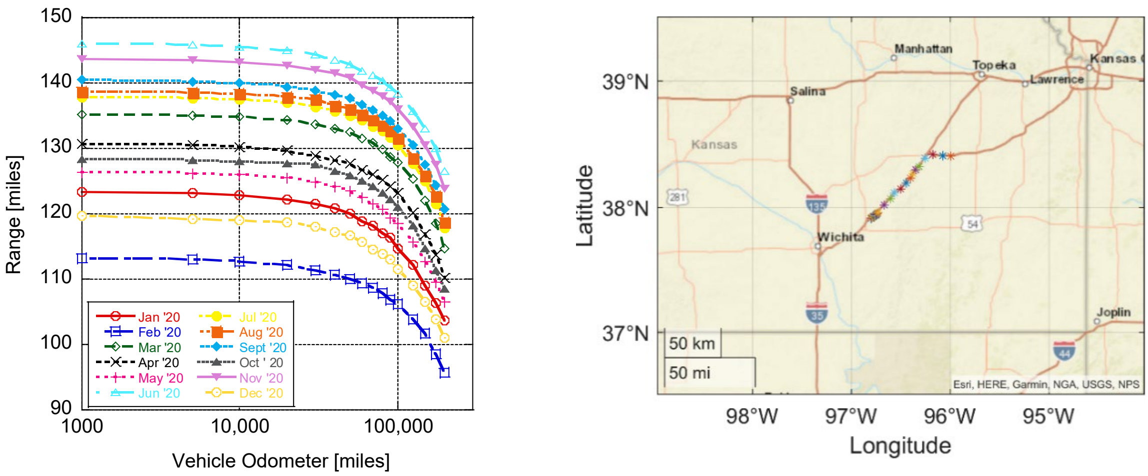

(**a**) (**b**)

Figure 15. (**a**) Range of Jaguar I-Pace on I-35 N starting from the Oklahoma border as a function of the time of year and number of miles on the odometer with the HVAC system turned on. (**b**) The respective stopping points of the first leg indicated by symbols * as the vehicle ages using January 2020 as the month.

Figure 15b demonstrates where the consumer would need to stop during the month of January as a function of vehicle age. As the odometer mileage increases, stops closer to Wichita, KS, would be needed. This could be problematic for the consumer if they are used to a particular stop location and do not pay attention to their EV losing range as it ages. It is also unknown whether each EV has its own factor in range projection that considers odometer mileage. If not, it is possible that the satisfaction of the consumer would subsequently decrease as the vehicle ages.

In comparison, Figure 16a illustrates that it only takes the Tesla Model S around 15,000 miles to lose 5% of its range, and at 100,000 miles, it has lost on average 28.1% of its initial range for that month. This result is due to the chosen NCA battery aging curve in Figure 8 having a more drastic loss in battery capacity with the number of battery cycles. This is assumed to be a function of the respective nickel level in the perceived battery chemistries. Adding nickel improves the overall capacity of the battery but leads to a proportional decrease in its performance during cycling [71]. Note that NCA batteries generally have $LiNi_{0.8}Co_{0.15}Al_{0.05}O_2$ chemistry, and this also explains why the NCM_{523} battery performs better cyclically than the NCM_{622} battery in Figure 8.

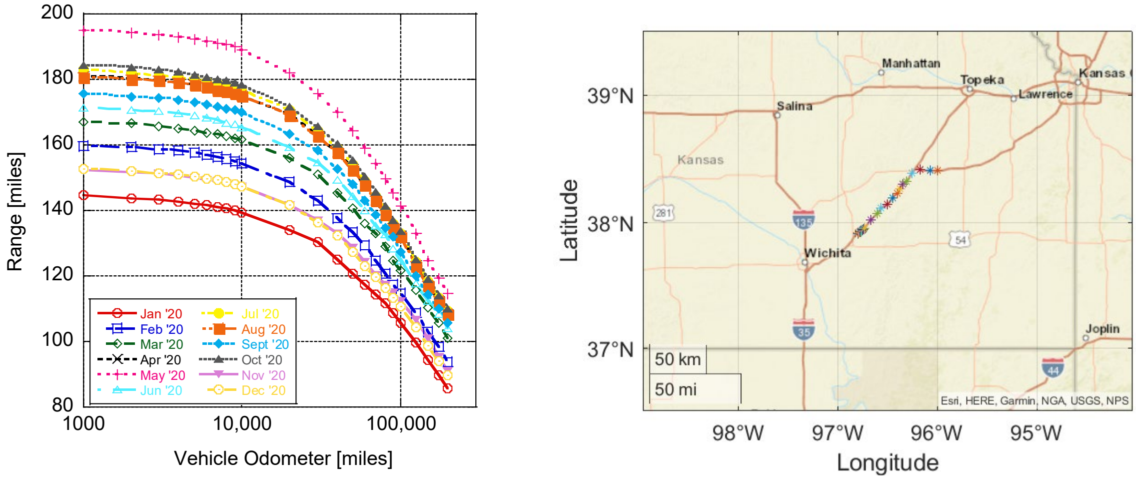

(**a**) (**b**)

Figure 16. (**a**) Range of Tesla Model S on I-35 S starting from Kansas City, MO, as a function of the time of year and number of miles on the odometer with the HVAC system turned on. (**b**) The respective stopping points of the first leg indicated by the symbols * as the vehicle ages using November 2020 as the month.

Now, at 100,000 miles, the average range over the year is 124.1 miles, which is a 53.1% decrease from its EPA-estimated 264.6 highway mile range. Furthermore, Figure 16b demonstrates a significant difference in stopping locations based on odometer mileage. In general, the layered ternary cathode materials of NCM and NCA batteries have a significantly high storage capacity and voltage potential, making them suitable for long-range EVs; however, they can have a poor rate capacity [72]. Thus, as shown here, the impact of battery aging can lead to significant losses in EV range, potentially worsening the range anxiety of the driver.

3.5. Rain and Snow

As indicated in the introduction, both rain and snow can lead to a respective increase in rolling resistance, subsequently impacting the range of an EV. In addition, the prior sections investigated high-speed corridors through the state of Kansas. Given the squared factor of velocity impacting drag in Equation (4), this will result in a greater loss in range in comparison to a lower-speed route. Thus, Figure 17a demonstrates the impact of rain on the range of a Tesla Model 3 during a lower-speed route (US-54 East). As indicated, the range of the vehicle generally falls linearly with the amount of rain on the road during July of 2020. Reviewing the stopping locations in Figure 17b shows, like age, that earlier stops are needed, and at the highest rain level on the road (0.10 inches), a third stop would be required before reaching the Missouri border.

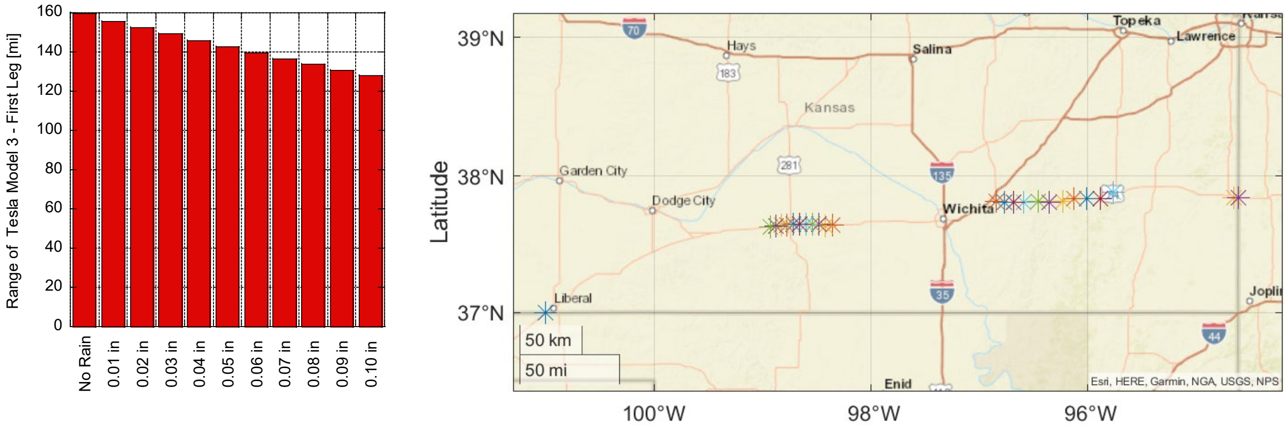

(**a**) (**b**)

Figure 17. (**a**) Range of Tesla Model 3 in July 2020 heading East on US-54 as a function of rain on road. (**b**) Stopping locations indicated by the symbols * based on rain level with sooner stops needed heading out of Liberal, KS. Vehicle mileage = 1000 miles, HVAC system on.

With respect to snow, Figure 18a demonstrates the range of the Tesla Model 3 heading West on US-54 with varying levels of fresh snow on the ground in February 2020. Like rain, the range of the EV drops linearly with the amount of snow cover. Now, three stops are needed for all scenarios to make it from the Missouri border to Liberal, KS, with snow having a significant impact on range, as shown in Figure 18b. Both the rain and snow results show that EVs might consider linking to local weather stations to obtain rainfall/snowfall data and modify their range predictions accordingly.

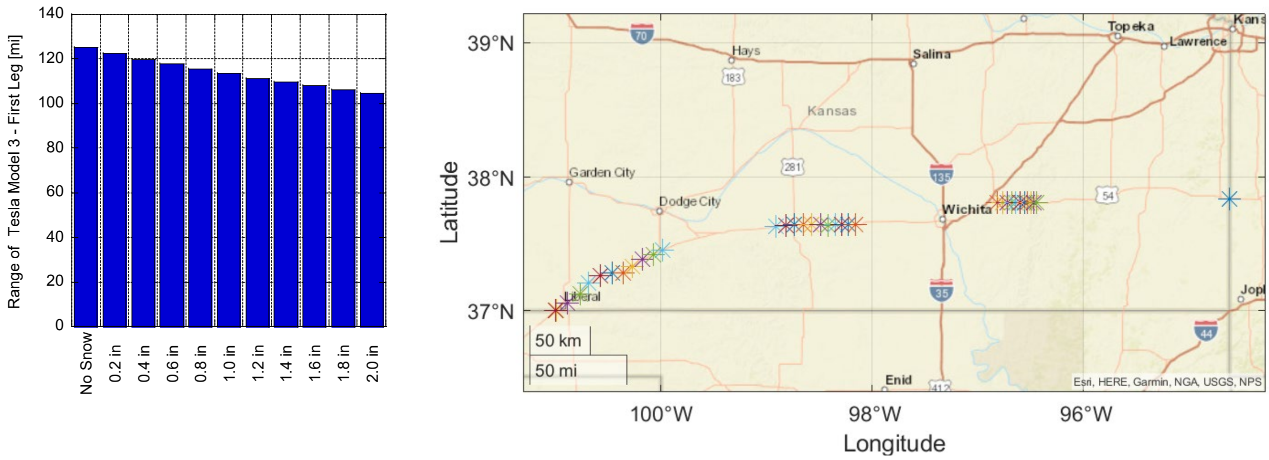

(**a**) (**b**)

Figure 18. (**a**) Range of Tesla Model 3 in February 2020 heading West on US-54 as a function of snow on road. (**b**) Stopping locations indicated by the symbols * based on snow level with sooner stops needed heading from the Missouri border. Vehicle mileage = 1000 miles, HVAC system on.

3.6. Model Exploration

The constructed model is believed to be the simplest version that captures all pertinent facets that impact EV driving range. As a final demonstration of its use, a vehicle comparison of the final state of charge driving on I-135 North and South is provided in Figure 19 for August of 2020 with the HVAC system engaged and the vehicle aged 50,000 miles. The total distance on this relatively short interstate route is 95.9 miles; hence, all vehicles, as indicated by the EPA, should be able to traverse this route without needing to stop. Furthermore, an illustration of the predictive capability of the model is provided by simulating the 2021

VW ID.4, for which only EPA data currently exist with the estimated parameters provided in Table A2. Like earlier efforts, the calibration procedure of the VW ID.4 with the HVAC system off was performed to try to match the MCT test results from the EPA (see Figure 20). Then, the same procedure as that used for the Tesla Model 3 was conducted to estimate the mileage of the vehicle as a function of ambient temperature with the HVAC system off and on. Like the VW Golf, the SOC_{min} and SOC_{max} had to be expanded to their maximum values to achieve close to the EPA-stated ranges and MPG_e. The values do deviate more than the other models due to the fact that it employs newer battery technology (NCM_{712}), but it was assumed here to have the NCM_{622} battery profiles, given the unavailability of literature data.

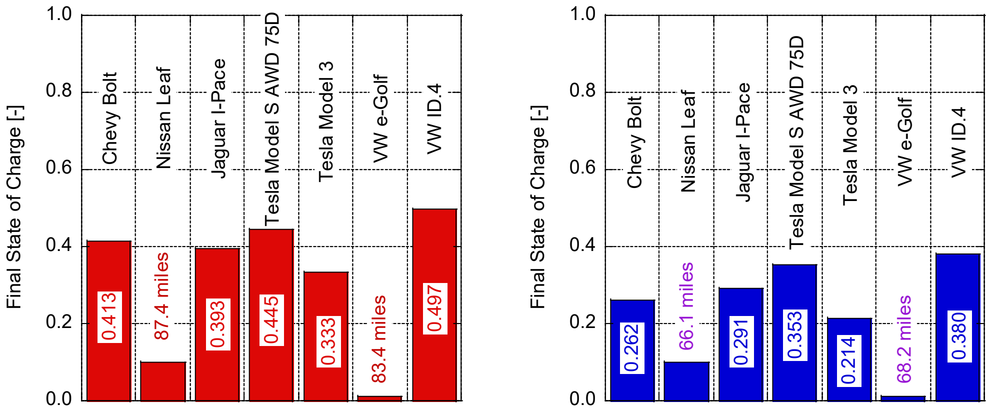

(**a**) (**b**)

Figure 19. Final state of charge of each vehicle or the vehicle range when driving from (**a**) Wichita, KS, to Salina, KS, or (**b**) Salina, KS, to Wichita, KS, on I-135 North and South, respectively, during August of 2020.

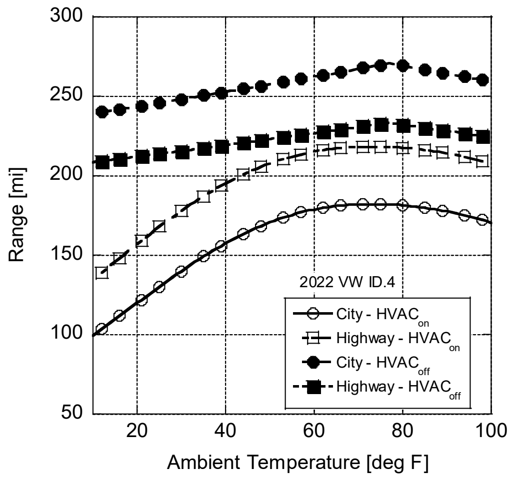

Figure 20. Estimated range of the 2022 VW ID.4 vehicle as a function of ambient temperature with the HVAC system off and on.

As indicated in Figure 19, not all vehicles can make the I-135 trip without recharging. All vehicles will need recharging in Wichita, KS, to make the 191.8-mile roundtrip journey. Interestingly, the VW ID.4 has the best range, likely due to the fact that it was estimated with newer battery chemistry. Thus, while battery technology continues to improve, it does seem that significant improvements are still needed to achieve the 300-mile range that has often been discussed as one barrier to commercial success [73]. Finally, it would be interesting to check the predictability of the VW ID.4 model once more data are available.

3.7. Predictive Spreadsheet

Given the relative complexity of the model for others to use and the need to translate the findings for widespread usage as part of planning, it was decided to extrapolate the findings into an Excel spreadsheet. To generate the spreadsheet, the six vehicles in Table A1 were simulated over the routes I-I35, US-54, I-70, and I-35 in both directions for each month in the year 2020. In addition, the influences of vehicle age (through mileage: m_i), the HVAC system (off and on), and the amount of rain on the road (t_{rt}) were included as variable parameters. From this information, an average range multiplier (R_{mult}) across all vehicles was determined, which can be used to modify the EPA-stated range of the vehicle. It was realized that the data for R_{mult} could be coalesced into a curve fit:

$$R_{mult} = (A + B \cdot t_{rt})\left(C + D \cdot m_i + E \cdot m_i^2 + F \cdot m_i \cdot t_{rt}\right) \tag{53}$$

Using Matlab's fmincon function, the values of A, B, C, D, E, and F were fit to each route, whether the HVAC system was on or off, and the month of the year. In comparison to the model results, the curve fit had around a 0.2% difference in R_{mult}. Figure 21 illustrates the input to the spreadsheet along with the model results. All the user must accomplish is to provide the EPA-stated range of the vehicle, the level of charge of the battery pack, the current mileage of the vehicle, whether the HVAC system is engaged, and whether there is rain on the road. The calibrated curve fit will then tell the user what the estimated range of that vehicle will be over the routes provided.

Questions	Input to Model	
What is the EPA stated range of the vehicle?	213	miles
What is the current battery pack charge level (0% - Empty; 100% - Full)	87%	
What is the mileage (aka odometer) of the vehicle?	49,000	miles
Is the HVAC system ON or OFF?	ON	
How much rain is on the road in inches?	0.05	inches

	Estimated Electric Vehicle Range in Miles based on Road Speed, Direction, and Ambient Conditions							
	I-135 North	I-135 South	US-54 East	US-54 West	I-70 East	I-70 West	I-35 North	I-35 South
Jan.	83.5	87.6	111.5	85.4	98.7	75.6	85.9	78.5
Feb.	78.5	94.0	103.7	90.5	95.4	80.6	78.4	85.4
Mar.	103.7	79.4	107.5	107.4	86.8	94.7	94.0	89.0
Apr.	102.5	82.8	103.0	114.1	84.5	100.8	90.5	95.5
May	99.6	88.9	100.9	119.8	84.9	105.7	87.3	102.3
June	113.4	81.6	115.4	113.0	91.8	99.7	101.7	92.3
July	107.4	86.3	109.8	116.5	90.2	103.0	95.9	97.6
Aug.	107.6	86.2	110.9	115.6	91.0	102.1	96.5	96.7
Sept.	107.1	84.0	112.2	112.7	90.9	99.0	97.0	93.5
Oct.	101.7	83.4	101.4	115.5	83.5	102.1	89.2	97.0
Nov.	103.7	79.3	118.0	98.2	94.7	86.3	99.8	81.9
Dec.	80.9	92.3	109.8	87.7	99.3	77.8	82.6	82.1

Figure 21. Inputs to the predictive spreadsheet and corresponding estimated range based on route and month of the year.

4. Discussion and Recommendations

The findings illustrate that the EPA should reconsider how they generate the range of EVs since range anxiety is a significant issue for the consumer. As illustrated, weather, speed, the age of the vehicle, and heating and air conditioning all play a significant role in decreasing the range of EVs. Thus, data should be taken at different temperatures to demonstrate the impact of the HVAC system. Moreover, a new driving profile more indicative of the speeds seen during highway driving is needed. Furthermore, estimates of the loss of range based on whether it is raining or snowing and the age of the vehicle should be provided to the consumer. It is critical that these advances in knowledge be portrayed to the consumer; otherwise, their attitudes towards EVs will change, and they will revert to using petroleum-based vehicles. For example, about 20% of early adopters in California have switched back, with their dissatisfaction with home charging being a primary factor [74]. The data illustrated here show that more charging events will be needed given current battery technology, thus potentially worsening the dissatisfaction of consumers.

5. Conclusions

Range anxiety continues to be a primary factor for consumers when considering the purchase of an EV. While numerous EVs now boast ranges greater than 200 miles based on EPA data generated from the SAE J1634 testing procedure, the actual range of the EV on the road can be significantly less. Weather, weight, road conditions and grade, and cabin conditioning all play a significant role in decreasing actual driving distance. To account for these facets, this effort endeavored to create the simplest model that accounts for all pertinent factors to generate a more realistic outcome of EV range.

The initial calibration of six commercial vehicles to the EPA-stated range data shows good accuracy, with the model deviating by only 0.45 and 0.57 miles for highway and city ranges, respectively. Of the six vehicles, five were estimated to have *SOC* ranges deemed suitable within research findings. Subsequently, predicting a Chevy Bolt using simulated chassis dynamometer tests shows only a 1–2% loss in range due to added weight or tire pressure. However, simulating the impact of road grade, wind, and vehicle speed in a true highway environment demonstrated significant losses of up to 43.2% of the EPA-stated range for a Nissan Leaf. In addition, ambient temperature effects resulted in the Leaf requiring around 2 $\times$ the number of charging events. Overall, model predictions indicate losses (city or highway) from 24.9–57.8% at 20 °F to 8.1–37.5% at 95 °F for the vehicles simulated.

Battery chemistry was also found to play a role in EV range as the vehicle ages. The simulated Jaguar I-Pace with an NCM_{622} battery had a 43.7% decrease in range at 100,000 miles, whereas the Tesla Model S with an NCA battery predicted a 53.1% decrease in range at the same vehicle mileage. Here, the greater decrease in capacity of the NCA battery with increasing cycles resulted in the Tesla losing a larger percentage of its range with mileage. The subsequent model expansion that was employed to include rain and snow data demonstrates different stopping locations along a lower speed route, which suggests that in-vehicle estimations of range might need to link to local weather stations to modify their algorithms. Model exploration and expansion to the VW ID.4 reveals that significant efforts are still needed in battery chemistry to achieve a true 300-mile on-road range for lower-cost EVs. It is recommended that the EPA reconsider their range estimations and provide more realistic values expected by the consumer given possible driving profiles in Kansas based on the time of year and the age of the vehicle. Finally, a relatively simple spreadsheet was created that allows users to quickly estimate the range of an electric vehicle based on the route, time of year, battery pack charge, age of the vehicle, whether the HVAC system is engaged, and whether rain is present.

Author Contributions: Conceptualization, C.D.; methodology, T.S., G.B., and C.D.; software, T.S., G.B., and C.D.; validation, T.S., G.B., and C.D.; formal analysis, T.S., G.B., A.W., and C.D.; investigation, T.S., G.B., A.W., and C.D.; resources, C.D.; data curation, T.S., G.B., and C.D.; writing—original draft preparation, C.D.; writing—review and editing, T.S., G.B., A.W., and C.D.; visualization, C.D.; supervision, C.D.; project administration, C.D.; funding acquisition, C.D. All authors have read and agreed to the published version of the manuscript.

Funding: This research was funded by the Kansas Department of Transportation, grant number KTRAN-KU-21-1.

Data Availability Statement: Not applicable.

Acknowledgments: We gratefully acknowledge the efforts of Allison Smith at the Kansas Department of Transportation for her help in improving the predictive nature of the model and her constant review of the material.

Conflicts of Interest: The authors declare no conflict of interest.

Nomenclature

Variable	Description	Units
a	Parameter in distance determination	[-]
a_{aux}, b_{aux}, c_{aux}	Auxiliary power draw parameters	[W], [W s m^{-1}], [W s^2 m^{-2}]
a_{EPA}, b_{EPA}, c_{EPA}	EPA rolling resistance and drag coefficients	[N], [N s m^{-1}], [N s^2 m^{-2}]
A, B, C, D, E, F	Parameters in range multiplier curve fit	[-], [in^{-1}], [-], [mi^{-1}], [mi^{-2}], [mi^{-1} in^{-1}]
A_f	Frontal area of vehicle	[m^2]
Ah	Battery pack capacity	[A h]
Ah^0	Initial capacity of battery pack	[A h]
a_{rr}, b_{rr}, c_{rr}	Rolling resistance parameters	[N], [N s m^{-1}], [N s^2 m^{-2}]
a_{rt}, b_{rt}, c_{rt}	Precipitation parameters for rolling resistance	[-], [m^{-1}], [s m^{-2}]
a_{YM}, b_{YM}, c_{YM}, d_{YM}, e_{YM}, f_{YM}	Energy consumption parameters for HVAC system on	[kWh mi^{-1}], [kWh mi^{-1} °F^{-1}], [kWh mi^{-1} °F^{-2}], [kWh mi^{-1} °F^{-3}], [kWh mi^{-1} °F^{-4}], [kWh mi^{-1} °F^{-5}]
c	Parameter in distance determination	[-]
C_D	Drag coefficient	[-]
c_m	Battery pack capacity multiplier	[-]
$C_{r,mult}$	Multiplier on nominal battery capacity	[-]
c_y	Battery pack cycles	[-]
d	Distance	[m]
D_{phase}	Distance of each phase of EPA test	[m]
E	Elevation	[m]
E_{aux}	Energy consumption per unit distance	[kWh mi^{-1}]
$ECdc_{cycle}$	Total energy consumption per unit distance	[W h m^{-1}]
$ECdc_{phase}$	Energy consumption per phase of EPA test	[W h m^{-1}]
Edc_{phase}	DC energy consumption per phase of EPA test	[W h]
F	Scaling factor on HVAC engaged models	[-]
F_D	Drag force	[N]
F_G	Gradation force	[N]
F_R	Rolling resistance force	[N]
F_T	Traction force	[N]
F_x	Acceleration or deceleration force	[N]
g	Standard gravity	[m s^{-2}]
GP	Maximum gradient of road	[deg]
i_0	Final drive gear ratio	[-]
i_g	Transmission gear ratio	[-]
I_{pack}	Pack amperage	[A]
I_{ref}	Reference amperage	[A]
I_t	Amperage of a single representative battery	[A]
K_{UDDS}	Scaling factor of UDDS cycle	[-]
K_{cycle}	Cycle scaling factor	[-]
K_{phase}	Phase scaling factor	[-]
lat	Latitude	[deg]
lon	Longitude of vehicle location	[deg]
m	Overall mass of vehicle	[kg]
m_i	Mileage of vehicle	[mi]
n	Time-step	[-]
N	Motor speed	[rev min^{-1}]
n_{cycle}	Number of cycles for EPA test	[-]
N_{par}	Number of batteries in parallel	[-]
P_{aux}	Auxiliary power draw	[W]
P_b	Brake power	[W]
P_m	Motor power	[W]
P_r	Regenerative braking power	[W]
p_{ref}	Reference pressure	[kPa]
p_{tire}	Tire pressure	[kPa]
q_{dr}	Map driving direction	[deg]
q_{wind}	Wind direction	[deg]

R_{cycle}	Range of EV for cycle	[m]
r_d	Tire radius	[m]
R_{Earth}	Radius of Earth	[m]
R_{mult}	Range multiplier	[-]
SOC	State of Charge	[-]
t	Time	[s]
T_{amb}	Ambient temperature	[K]
T_{ref}	Reference temperature	[K]
t_{rt}	Thickness of rain or snow	[m]
T_t	Battery pack temperature	[K]
UBE	Total usable battery energy	[W h]
U_w	Wind speed in x-direction	[m s^{-1}]
V	Current vehicle velocity	[m s^{-1}]
$\overline{V}$	Average vehicle velocity	[m s^{-1}]
V_{cabin}	Cabin volume	[m^3]
V_{eff}	Effective vehicle velocity	[m s^{-1}]
V_{pack}	Current pack voltage	[VDC]
$\overline{V}_{pack}$	Average pack voltage over time step	[VDC]
V_w	Wind speed in y-direction	[m s^{-1}]
V_{wind}	Wind speed	[m s^{-1}]
x	Parameter in bearing calculation	[-]
y	Parameter in bearing calculation	[-]
Z_{ref}	Reference weight	[N]

Greek Variables

Variable	Description	Units
α	Tire pressure exponent for rolling resistance	[-]
α_{aux}	Temperature exponential factor for HVAC system off	[-]
β	Weight exponent for rolling resistance	[-]
β_{br}	Bearing angle	[deg]
γ,χ,δ	Capacity offset parameters	[W], [-], [-]
ΔAh	Battery pack capacity change	[A h]
Δf	Difference in latitude between time steps	[deg]
Δl	Difference in longitude between time steps	[deg]
Δt	Time step	[s]
ΔWh	Change in battery pack energy	[W h]
h_m	Motor efficiency	[-]
h_t	Driveline efficiency	[-]
φ	Yaw angle of the vehicle	[rad]
ϑ	Angle of wind relative to direction of motion	[rad]
θ	Roadway slope	[deg]
ρ	Density of air	[kg m^{-3}]
μ_r	Rolling resistance coefficient	[-]
τ_b	Brake torque	[N m]
τ_w	Wheel torque	[N m]

Acronyms

AAA	American Automobile Association
CSC	Constant Speed Cycle
E	East
EPA	Environmental Protection Agency
EV	Electric Vehicle
GPS	Global Positioning System
HVAC	Heating, Ventilation, and Air Conditioning
HWFET	Highway Fuel Economy Test
MCT	Multi-Cycle Test
MPG_e	Miles Per Gallon Equivalent
N	North
NCA	Nickel Cobalt Aluminum Oxide
NCM_{333}	$LiNi_{1/3}Co_{1/3}Mn_{1/3}O_2$
NCM_{523}	$LiNi_{0.5}Co_{0.2}Mn_{0.3}O_2$
NCM_{622}	$LiNi_{0.6}Co_{0.2}Mn_{0.2}O_2$
NEDC	New European Driving Cycle
S	South
SAE	Society of Automotive Engineers
UDDS	Urban Dynamometer Driving Schedule
US06	Supplemental Federal Test Procedure
W	West

Appendix A

Table A1. Pertinent vehicle parameters for six commercial EVs.

Vehicle and Model Year	**2017–2019 Chevy Bolt**	**2018–2020 Nissan Leaf**	**2019 Jaguar I-Pace**	**2019 Tesla Model S AWD 75D**	**2019 Tesla Model 3 Std. Range RWD**	**2019 VW e-Golf**
AAA Test Data Available	Yes	Yes	No	Yes	No	Yes
Coefficient of Drag [-]	0.32	0.28	0.29	0.24	0.23	0.25
Vehicle Height [in]	62.8	61.6	61.3	56.5	56.8	58.3
Vehicle Width [in]	69.5	70.5	74.6	77.3	72.8	70.8
Frontal Area [m^2]	2.211	2.162	2.315	2.026	1.984	2.048
Vehicle Mass [kg]	1616	1557	2140	2215	1611	1585
Unloaded Tire Diameter [in]	25.5	24.9	29.6	27.7	29.4	24.9
Tire pressure [psi]	38	36	37	45	37	41
Tire Revolutions per Mile [rev min^{-1}]	815	836	703	751	708	836
Final Drive Ratio [-]	7.05	8.19	9.06	9.73	9	9.75
Motor Type	Permanent Magnet Synchronous A	Permanent Magnet Synchronous B	Permanent Magnet Synchronous B	AC Induction	Permanent Magnet Synchronous B	Permanent Magnet Synchronous B
Maximum Motor Speed [rev min^{-1}]	8810	10,390	13,000	18,000	13,800	12,000
Maximum Brake Torque [N-m]	360	321	696	658	431	290
Maximum Brake Power [kW]	150	110	296	386	211	100
Maximum Regeneration Power [kW]	60	43.3	116.5 *	60	116.5 *	70

Table A1. *Cont.*

Vehicle and Model Year	2017–2019 Chevy Bolt	2018–2020 Nissan Leaf	2019 Jaguar I-Pace	2019 Tesla Model S AWD 75D	2019 Tesla Model 3 Std. Range RWD	2019 VW e-Golf
Maximum Speed [mi hr^{-1}]	91	89.5	124	139.8	130	93.2
Cabin Volume [ft^3]	94.4	116.0	102.6	94	97	93.5
Battery Chemistry [-]	NCM_{622}	NCM_{523}	NCM_{622}	NCA_1	NCA_2	NCM
Batteries in Series [-]	96	96	108	96	96	88
Batteries in Parallel [-]	3	2	4	74	46	3
Nominal Pack Voltage [VDC]	350	350	388	400	350	370
Nominal Pack Capacity [Ah]	171.4	115	222.9	245	230	111
Calculated Pack Capacity [kW-hr]	59.99	40.25	86.49	98.00	80.50	41.07
Initial Cycles for EPA Tests [-]	4	6	4	6	4	8
$SOC_{\min}/SOC_{\max}$	0.1/0.8305	0.1/0.9071	0.1/0.8664	0.1/0.8298	0.1/0.8571	0.01/0.9946
EPA City/Highway [mi]	255.1/217.4	165.2/132.4	244.8/220.8	255.0/264.6	230.5/206.3	130.6/117.9
Model City/Highway [mi]	254.6/218.0	165.3/132.5	244.8/220.7	255.6/265.1	229.6/205.7	131.2/116.4
Unadjusted MPG_e City/Highway	182.2/157.4	177.3/142.1	114.1/102.9	137.9/142.7	138.2/123.8	126.0/111.0
Model MPG_e City/Highway	182.9/156.6	177.3/142.1	114.1/102.9	137.9/143.0	138.2/123.8	125.7/111.5
HVAC Off 20 °F and 95 °F City/Highway Loss [mi]	−31/−15 −6/−2	−19/−9 −2/−2	N/A	−32/−21 −19/−14	N/A	−13/−3 −7/0
HVAC Off Model 20 °F and 95 °F City/Highway Loss [mi]	−28.6/−16.2 −9.4/−5.1	−17.3/−10.9 −5.6/−3.5	−31.4/−25.5 −10.6/−8.5	−31.5/−27.3 −10.6/−9.0	−24.8/21.4 −8.2/−7.0	−10.0/−7.7 −3.3/−2.5
HVAC On 20 °F and 95 °F City/Highway Loss [mi]	−148/−68 −65/−22	−58/−26 −24/−8	N/A	−109/−69 −48/−25	N/A	−65/−20 −34/−9
HVAC On Model 20 °F and 95 °F City/Highway Loss [mi]	−145.1/−74.5 −69.5/−17.6	−50.3/−33.0 −21.2/−13.3	−95.1/−62.2 −53.8/−24.5	−99.4/−75.7 −48.2/−25.1	−132.8/−86.1 −86.1/−20.8	−50.5/−29.2 −30.2/−10.8
$C_{r,mult}$	1.0428	1.0596	1.0428	0.9045	0.9884	0.9012
γ	0.8786	0.9222	0.8786	0.8851	1.0069	0.8861
χ	1.0391	1.0592	1.0391	1.0095	1.0552	1.0042
δ **	0	0	0	1.7714	0	0.4936
a_{EPA} [N]	63.1648	37.0537	−62.1995	−6.6723	77.3991	−27.6012
b_{EPA} [N s m^{-1}]	0.4020	1.2567	2.8080	0.1171	−1.4856	0.4535
c_{EPA} [N s^2 m^{-2}]	0.4300	0.4296	0.4108	0.3470	0.3653	0.3860
a_{rr} [N]	5.0165×10^{-2}	2.9817×10^{-2}	-3.8378×10^{-2}	-4.2681×10^{-3}	6.1051×10^{-2}	-2.2877×10^{-2}
b_{rr} [N s m^{-1}]	3.1937×10^{-4}	1.0114×10^{-3}	1.7326×10^{-3}	7.3551×10^{-5}	-1.1702×10^{-3}	3.7573×10^{-4}
c_{rr} [N s^2 m^{-2}]	8.9076×10^{-6}	5.7334×10^{-5}	8.2824×10^{-6}	3.7951×10^{-5}	7.5030×10^{-5}	6.8783×10^{-5}
a_{aux} [W]–HVAC off	9.6491×10^{2}	6.2301×10^{2}	1.5011×10^{3}	1.8325×10^{3}	1.2063×10^{3}	3.6632×10^{2}
b_{aux} [W s m^{-1}]–HVAC off	6.1117×10^{1}	7.1905×10^{1}	1.4680×10^{2}	1.4651×10^{2}	5.9168	3.9827×10^{2}
c_{aux} [W s^2 m^{-2}]–HVAC off	1.5524	3.6700	1.0389×10^{1}	4.0367	1.1617×10^{1}	1.0023
α_{aux}–HVAC off	2.3446	2.2228	1.8577	1.6729	1.8577	1.0136
Heating System	Resistance	Heat Pump	Heat Pump	Resistance	Resistance	Heat Pump
a_{aux} [W]–HVAC on	3.1176×10^{1}	6.2800	6.1403	1.7323×10^{1}	1.3458×10^{1}	9.9413
b_{aux} [W s m^{-1}]–HVAC on	6.1308×10^{-1}	7.1900×10^{-1}	3.4647×10^{-1}	1.3758×10^{0}	6.3044×10^{-1}	4.3196×10^{-1}

Table A1. *Cont.*

Vehicle and Model Year	2017–2019 Chevy Bolt	2018–2020 Nissan Leaf	2019 Jaguar I-Pace	2019 Tesla Model S AWD 75D	2019 Tesla Model 3 Std. Range RWD	2019 VW e-Golf
c_{aux} [W s^2 m^{-2}]–HVAC on	9.0834×10^{-3}	3.6300×10^{-2}	2.2299×10^{-2}	1.3437×10^{-2}	6.8909×10^{-3}	3.1307×10^{-2}
a_{YM} [kWh mi^{-1}]	1.3088×10^{-1}	1.3801×10^{-1}	4.0411×10^{-1}	1.4360×10^{-1}	3.2757×10^{-1}	2.4480×10^{-1}
b_{YM} [kWh mi^{-1} °F^{-1}]	-3.5724×10^{-3}	-3.4800×10^{-3}	-7.5055×10^{-3}	-3.2636×10^{-3}	-8.1276×10^{-3}	-3.7500×10^{-3}
c_{YM} [kWh mi^{-1} °F^{-2}]	4.6682×10^{-5}	5.1000×10^{-5}	9.5581×10^{-5}	4.7516×10^{-5}	1.1177×10^{-4}	4.2937×10^{-5}
d_{YM} [kWh mi^{-1} °F^{-3}]	-2.4521×10^{-7}	-2.8300×10^{-7}	-4.9901×10^{-7}	-2.7221×10^{-7}	-6.0641×10^{-7}	-2.2862×10^{-7}
e_{YM} [kWh mi^{-1} °F^{-4}]	3.3140×10^{-11}	1.4500×10^{-10}	2.9917×10^{-10}	2.7485×10^{-10}	2.7688×10^{-10}	3.2365×10^{-10}
f_{YM} [kWh mi^{-1} °F^{-5}]	3.9879×10^{-12}	2.8400×10^{-12}	8.1332×10^{-12}	2.1291×10^{-12}	7.5301×10^{-12}	4.5652×10^{-12}

* Estimates and ** Not enough data to calibrate the parameter.

Table A2. Parameters for the 2021 VW ID.4.

Coefficient of Drag [-]	0.28
Vehicle Height [in]	64.4
Vehicle Width [in]	72.9
Frontal Area [m^2]	2.18 *
Vehicle Mass [kg]	2049
Unloaded Tire Diameter [in]	29.2
Tire pressure [psi]	50
Tire Revolutions per Mile [rev min^{-1}]	692
Final Drive Ratio [-]	12.99
Motor Type	Permanent Magnet Synchronous B
Maximum Motor Speed [rev min^{-1}]	16,000
Maximum Brake Torque [N−m]	309
Maximum Brake Power [kW]	150
Maximum Regeneration Power [kW]	70 *
Maximum Speed [mi hr^{-1}]	99.4
Cabin Volume [ft^3]	99.9
Battery Chemistry [-]	NCM_{712} (used NCM_{622} data)
Batteries in Series [-]	96
Batteries in Parallel [-]	3
Nominal Pack Voltage [VDC]	400
Nominal Pack Capacity [Ah]	205
Calculated Pack Capacity [kW−hr]	82
Initial Cycles for EPA Tests [-]	4
$SOC_{\min}/SOC_{\max}$	0.1/0.9999
EPA City/Highway [mi]	278.5/237.1
Model City/Highway [mi]	270.8/233.4
Unadjusted MPG_e City/Highway	107/91

Table A2. *Cont.*

Model MPG$_e$ City/Highway	120.8/104.1
HVAC Off 20 °F and 95 °F City/Highway Loss [mi]	N/A
HVAC Off Model 20 °F and 95 °F City/Highway Loss [mi]	−27.7/−21.4 −9.0/−6.6
HVAC On 20 °F and 95 °F City/Highway Loss [mi]	N/A
HVAC On Model 20 °F and 95 °F City/Highway Loss [mi]	−151.0/−76.4 −96.4/−22.2
$C_{r,mult}$	1.0428
γ	0.8786
χ	1.0391
δ**	0
a_{EPA} [N]	65.0997
b_{EPA} [N s m^{-1}]	1.8644
c_{EPA} [N s^2 m^{-2}]	0.4068
a_{rr} [N]	4.6304×10^{-2}
b_{rr} [N s m^{-1}]	1.3246×10^{-3}
c_{rr} [N s^2 m^{-2}]	3.2345×10^{-5}
a_{aux} [W]–HVAC off	1.3973×10^{3}
b_{aux} [W s m^{-1}]–HVAC off	8.0243×10^{-1}
c_{aux} [W s^2 m^{-2}]–HVAC off	1.2360×10^{1}
α_{aux}–HVAC off	1.8577
Heating System	Resistance
a_{aux} [W]–HVAC on	9.9394
b_{aux} [W s m^{-1}]–HVAC on	4.6607×10^{-1}
c_{aux} [W s^2 m^{-2}]–HVAC on	5.0793×10^{-3}
a_{YM} [kWh mi^{-1}]	4.7395×10^{-1}
b_{YM} [kWh mi^{-1} °F^{-1}]	-1.1758×10^{-2}
c_{YM} [kWh mi^{-1} °F^{-2}]	1.6167×10^{-4}
d_{YM} [kWh mi^{-1} °F^{-3}]	-8.7681×10^{-7}
e_{YM} [kWh mi^{-1} °F^{-4}]	3.9058×10^{-10}
f_{YM} [kWh mi^{-1} °F^{-5}]	1.0961×10^{-11}

* Estimates and ** Not enough data to calibrate the parameter.

References

1. Pevec, D.; Babic, J.; Carvalho, A.; Ghiassi-Farrokhfal, Y.; Ketter, W.; Podobnik, V. A survey-based assessment of how existing and potential electric vehicle owners perceive range anxiety. *J. Clean. Prod.* **2020**, *276*, 122779. [CrossRef]
2. Analytics Team. Survey: Electric Vehicles' Range Jumps to Top of Priorities for Consumers. Available online: https://www.autolist.com/news-and-analysis/2021-survey-electric-vehicles (accessed on 1 June 2022).
3. Voelcker, J. How Much Electriccar Range Is 'Enough'? 300 Miles Much Better Than 200 Miles: Survey. Available online: https://www.greencarreports.com/news/1112298_how-much-electric-car-range-is-enough-300-miles-much-better-than-200-miles-survey (accessed on 1 June 2022).
4. Performance, L.D.V.; Committee, E.M. *Battery Electric Vehicle Energy Consumption and Range Test Procedure*; SAE International: Warrendale, PA, USA, 2017. [CrossRef]

5. Hu, K.; Wu, J.; Schwanen, T. Differences in Energy Consumption in Electric Vehicles: An Exploratory Real-World Study in Beijing. *J. Adv. Transp.* **2017**, *2017*, 4695975. [CrossRef]
6. Hao, X.; Wang, H.; Lin, Z.; Ouyang, M. Seasonal effects on electric vehicle energy consumption and driving range: A case study on personal, taxi, and ridesharing vehicles. *J. Clean. Prod.* **2020**, *249*, 119403. [CrossRef]
7. Ahn, Y.; Yeo, H. An Analytical Planning Model to Estimate the Optimal Density of Charging Stations for Electric Vehicles. *PLoS ONE* **2015**, *10*, e0141307. [CrossRef]
8. Samenow, J. Blowing Hard: The Windiest Time of Year and Other Fun Facts on Wind. 2016. Available online: https://www.washingtonpost.com/news/capital-weather-gang/wp/2014/03/26/what-are-the-windiest-states-and-cities-what-is-d-c-s-windiest-month/ (accessed on 1 June 2022).
9. Lin, X.; Harrington, J.; Ciampitti, I.; Gowda, P.; Brown, D.; Kisekka, I. Kansas Trends and Changes in Temperature, Precipitation, Drought, and Frost-Free Days from the 1890s to 2015. *J. Contemp. Water Res. Educ.* **2017**, *162*, 18–30. [CrossRef]
10. Weiss, M.; Cloos, K.C.; Helmers, E. Energy efficiency trade-offs in small to large electric vehicles. *Environ. Sci. Eur.* **2020**, *32*, 46. [CrossRef]
11. Liu, K.; Yamamoto, T.; Morikawa, T. Impact of road gradient on energy consumption of electric vehicles. *Transp. Res. Part D Transp. Environ.* **2017**, *54*, 74–81. [CrossRef]
12. Al-Wreikat, Y.; Serrano, C.; Sodré, J.R. Driving behaviour and trip condition effects on the energy consumption of an electric vehicle under real-world driving. *Appl. Energy* **2021**, *297*, 117096. [CrossRef]
13. Pavlat, J.W.; Diller, R.W. An energy management system to improve electric vehicle range and performance. *IEEE Aerosp. Electron. Syst. Mag.* **1993**, *8*, 3–5. [CrossRef]
14. Sarrafan, K.; Muttaqi, K.M.; Sutanto, D.; Town, G.E. A Real-Time Range Indicator for EVs Using Web-Based Environmental Data and Sensorless Estimation of Regenerative Braking Power. *IEEE Trans. Veh. Technol.* **2018**, *67*, 4743–4756. [CrossRef]
15. Yi, Z.; Bauer, P.H. Effects of environmental factors on electric vehicle energy consumption: A sensitivity analysis. *IET Electr. Syst. Transp.* **2017**, *7*, 3–13. [CrossRef]
16. Tang, L.; Wei, S.; Valentage, J.; Li, Z.; Nair, S. Tire Pressure Impact on EV Driving Range. Available online: https://www.sae.org/news/2020/10/tire-pressure-impact-on-ev-driving-range (accessed on 1 June 2022).
17. Tannahill, V.R.; Muttaqi, K.M.; Sutanto, D. Driver alerting system using range estimation of electric vehicles in real time under dynamically varying environmental conditions. *IET Electr. Syst. Transp.* **2016**, *6*, 107–116. [CrossRef]
18. Laurikko, J.; Granström, R.; Haakana, A. Assessing Range and Performance of Electric Vehicles in Nordic Driving Conditions—Project "RekkEVidde". *World Electr. Veh. J.* **2012**, *5*, 45–50. [CrossRef]
19. Sarrafan, K.; Sutanto, D.; Muttaqi, K.M.; Town, G. Accurate range estimation for an electric vehicle including changing environmental conditions and traction system efficiency. *IET Electr. Syst. Transp.* **2017**, *7*, 117–124. [CrossRef]
20. Samadani, E.; Fraser, R.; Fowler, M. *Evaluation of Air Conditioning Impact on the Electric Vehicle Range and Li-Ion Battery Life*; SAE International: Warrendale, PA, USA, 2014. [CrossRef]
21. Horrein, L.; Bouscayrol, A.; Lhomme, W.; Dépature, C. Impact of Heating System on the Range of an Electric Vehicle. *IEEE Trans. Veh. Technol.* **2017**, *66*, 4668–4677. [CrossRef]
22. Szumska, E.M.; Jurecki, R.S. Parameters Influencing on Electric Vehicle Range. *Energies* **2021**, *14*, 4821. [CrossRef]
23. Mruzek, M.; Gajdáč, I.; Kučera, L'.; Barta, D. Analysis of Parameters Influencing Electric Vehicle Range. *Procedia Eng.* **2016**, *134*, 165–174. [CrossRef]
24. Depcik, C.; Gaire, A.; Gray, J.; Hall, Z.; Maharjan, A.; Pinto, D.; Prinsloo, A. Electrifying Long-Haul Freight-Part II: Assessment of the Battery Capacity. *SAE Int. J. Commer. Veh.* **2019**, *12*, 87–102. [CrossRef]
25. Kadijk, G.; Ligterink, N. *Road Load Determination of Passenger Cars*; TNO 2012 R10237; TNO: The Hague, The Netherlands, 2012.
26. United States Environmental Protection Agency. Data on Cars used for Testing Fuel Economy. Available online: https://www.epa.gov/compliance-and-fuel-economy-data/data-cars-used-testing-fuel-economy (accessed on 21 September 2021).
27. SketchAndCalc. Area Calculator. 2021. Available online: https://www.sketchandcalc.com/ (accessed on 1 June 2022).
28. Prša, A.; Harmanec, P.; Torres, G.; Mamajek, E.; Asplund, M.; Capitaine, N.; Christensen-Dalsgaard, J.; Depagne, É.; Haberreiter, M.; Hekker, S.; et al. Nominal values for selected solar and planetary quantities: Iau 2015 resOLUTION B3. *Astron. J.* **2016**, *152*, 41. [CrossRef]
29. Sinnott, R.W. Virtues of the Haversine. *Sky Telesc.* **1984**, *68*, 158.
30. National Oceanic and Atmospheric Administration. U.S. Wind Climatology. Available online: https://www.ncdc.noaa.gov/societal-impacts/wind/v-comp/202007 (accessed on 1 June 2022).
31. Hausmann, A.; Depcik, C. A Cost-Effective Alternative to Moving Floor Wind Tunnels in Order to Calculate Rolling Resistance and Aerodynamic Drag Coefficients. *SAE Int. J. Passeng. Cars Mech. Syst.* **2014**, *7*, 703–713. [CrossRef]
32. Grover, P.S. *Modeling of Rolling Resistance Test Data*; SAE International: Warrendale, PA, USA, 1998. [CrossRef]
33. Fechtner, H.; Teschner, T.; Schmuelling, B. Range prediction for electric vehicles: Real-time payload detection by tire pressure monitoring. In Proceedings of the 2015 IEEE Intelligent Vehicles Symposium (IV), Seoul, Korea, 28 June–1 July 2015; pp. 767–772. [CrossRef]
34. Ejsmont, J.; Sjögren, L.; Świeczko-Żurek, B.; Ronowski, G. Influence of Road Wetness on Tire-Pavement Rolling Resistance. *J. Civ. Eng. Archit.* **2015**, *9*, 1302–1310. [CrossRef]

35. Kihlgren, B.; Trafikinstitut, S.V.-O. *Flygplanshjuls Rullmotstånd I Torr Nysnö*; Statens väg-och Trafikinstitut: Linköping, Sweden, 1977.
36. Páscoa, J.C.; Brójo, F.P.; Santos, F.C.; Fael, P.O. An innovative experimental on-road testing method and its demonstration on a prototype vehicle. *J. Mech. Sci. Technol.* **2012**, *26*, 1663–1670. [CrossRef]
37. Pauwelussen, J. *Essentials of Vehicle Dynamics*; Elsevier Science: Amsterdam, The Netherlands, 2014.
38. American Association of State Highway and Transportation Officials. *A Policy on Geometric Design of Highways and Streets*; American Association of State Highway and Transportation Officials: Washington, DC, USA, 2001; Available online: https://law.resource.org/pub/us/cfr/ibr/001/aashto.green.2001.pdf (accessed on 1 June 2022).
39. Momen, F.; Rahman, K.M.; Son, Y.; Savagian, P. Electric Motor Design of General Motors' Chevrolet Bolt Electric Vehicle. *SAE Int. J. Altern. Powertrains* **2016**, *5*, 286–293. [CrossRef]
40. Burress, T. Benchmarking State-of-the-Art Technologies. 2013. Available online: https://www.energy.gov/sites/prod/files/2014/03/f13/ape006_burress_2013_o.pdf (accessed on 1 June 2022).
41. Staton, D.; Goss, J. Open Source Electric Motor Models for Commercial EV & Hybrid Traction Motors. In Proceedings of the CWIEME Berlin, Berlin, Germany, 20–22 June 2017.
42. Larsson, M. *Electric Motors for Vehicle Propulsion*; Linköpings Universitet: Linköping, Sweden, 2014.
43. Evtimov, I.; Ivanov, R.; Sapundjiev, M. Energy consumption of auxiliary systems of electric cars. *MATEC Web Conf.* **2017**, *133*, 06002. [CrossRef]
44. American Automobile Association, I. AAA Electric Vehicle Range Testing. 2019. Available online: https://www.aaa.com/AAA/common/AAR/files/AAA-Electric-Vehicle-Range-Testing-Report.pdf (accessed on 1 June 2022).
45. U.S. Department of Energy. Download Fuel Economy Data. Available online: https://www.fueleconomy.gov/feg/download.shtml (accessed on 1 June 2022).
46. Yuksel, T.; Michalek, J.J. Effects of Regional Temperature on Electric Vehicle Efficiency, Range, and Emissions in the United States. *Environ. Sci. Technol.* **2015**, *49*, 3974–3980. [CrossRef]
47. Hausmann, A.; Depcik, C. Expanding the Peukert Equation for Battery Capacity Modeling Through Inclusion of a Temperature Dependency. *J. Power Sources* **2013**, *235*, 148–158. [CrossRef]
48. O'Malley, R.; Liu, L.; Depcik, C. Comparative study of various cathodes for lithium ion batteries using an enhanced Peukert capacity model. *J. Power Sources* **2018**, *396*, 621–631. [CrossRef]
49. Samsung. Introduction of Samsung SDI's 94 Ah Cells. 2015. Available online: https://files.gwl.eu/inc/_doc/attach/StoItem/7213/Samsung_SDI_94Ah_Datasheet.pdf (accessed on 1 June 2022).
50. Kwon, S.-J.; Lee, S.-E.; Lim, J.-H.; Choi, J.; Kim, J. Performance and Life Degradation Characteristics Analysis of NCM LIB for BESS. *Electronics* **2018**, *7*, 406. [CrossRef]
51. Panasonic. Lithium Ion NCR18650B. 2021. Available online: https://www.batteryspace.com/prod-specs/NCR18650B.pdf (accessed on 1 June 2022).
52. ZeroAir.org. LiionWholesale Samsung 50e 21700 Li-Ion Cell Review. Available online: https://zeroair.org/2018/11/13/liionwholesale-samsung-50e-21700-li-ion-cell-review/ (accessed on 1 June 2022).
53. Saxena, S.; Le Floch, C.; MacDonald, J.; Moura, S. Quantifying EV battery end-of-life through analysis of travel needs with vehicle powertrain models. *J. Power Sources* **2015**, *282*, 265–276. [CrossRef]
54. Environmental Protection Agency. Title 40—Protection of Environment: Appendix IV to Part 86—Durability Driving Schedules. 2011. Available online: https://www.govinfo.gov/content/pkg/CFR-2011-title40-vol19/pdf/CFR-2011-title40-vol19-part86-appIV.pdf (accessed on 1 June 2022).
55. United States Council for Automotive Research LLC. USABC Electric Vehicle Battery Test Procedures Manual. 1996. Available online: https://avt.inl.gov/sites/default/files/pdf/battery/usabc_manual_rev2.pdf (accessed on 1 June 2022).
56. Bokare, P.; Maurya, A. Acceleration-deceleration behaviour of various vehicle types. *Transp. Res. Procedia* **2017**, *25*, 4733–4749. [CrossRef]
57. Proctor, C.L.; Grimes, W.D.; Fournier, D.J., Jr.; Rigol, J., Jr.; Sunseri, M.G. Analysis of acceleration in passenger cars and heavy trucks. *SAE Trans.* **1995**, *104*, 283–324. [CrossRef]
58. Kleeman, P. A fresh look at predicting carbon monoxide impacts at highway intersections. In Proceedings of the Transport Research Board A1 FC03-AIF06 Joint Summer Meeting, Ann Arbor, MI, USA, 11–15 January 1998.
59. Akçelik, R.; Besley, M. Acceleration and deceleration models. In Proceedings of the 23rd Conference of Australian Institutes of Transport Research (CAITR 2001), Melbourne, Australia, 10 December 2001; p. 12.
60. Bennett, C.; Dunn, R. Driver Deceleration Behaviour on a Motorway in New Zealand. *Transp. Res. Rec. J. Transp. Res. Board* **1995**, *1510*, 70–74. Available online: https://onlinepubs.trb.org/Onlinepubs/trr/1995/1510/1510-009.pdf (accessed on 1 June 2022).
61. Wang, J.; Dixon, K.K.; Li, H.; Ogle, J. Normal deceleration behavior of passenger vehicles at stop sign–controlled intersections evaluated with in-vehicle Global Positioning System data. *Transp. Res. Rec.* **2005**, *1937*, 120–127. [CrossRef]
62. Maurya, A.K.; Bokare, P.S. Study of Deceleration Behaviour of Different Vehicle Types. *Int. J. Traffic Transp. Eng.* **2012**, *2*, 253–270. [CrossRef]
63. Kostopoulos, E.D.; Spyropoulos, G.C.; Kaldellis, J.K. Real-world study for the optimal charging of electric vehicles. *Energy Rep.* **2020**, *6*, 418–426. [CrossRef]

64. Mannering, F.L. Effects of Interstate Speed Limits on Driving Speeds: Some New Evidence. In Proceedings of the Transportation Research Board 86th Annual Meeting, Washington, DC, USA, 21–25 January 2007; pp. 7–120.
65. De Leonardis, D.; Huey, R.; Green, J. *National Traffic Speeds Survey III: 2015*; DOT HS 812 485; National Highway Traffic Safety Administration: Washington, DC, USA, 2018. Available online: https://www.nhtsa.gov/sites/nhtsa.gov/files/documents/812485_national-traffic-speeds-survey-iii-2015.pdf (accessed on 30 June 2022).
66. AAA Foundation for Traffic Safety. *2019 Traffic Safety Culture Index*; AAA Foundation for Traffic Safety: Washington, DC, USA, 2020. Available online: https://aaafoundation.org/wp-content/uploads/2020/06/2019-Traffic-Safety-Culture-Index.pdf (accessed on 30 June 2022).
67. Argue, C. To What Degree Does Temperature Impact EV Range? Available online: https://www.geotab.com/blog/ev-range/ (accessed on 1 June 2022).
68. Bellocchi, S.; Leo Guizzi, G.; Manno, M.; Salvatori, M.; Zaccagnini, A. Reversible heat pump HVAC system with regenerative heat exchanger for electric vehicles: Analysis of its impact on driving range. *Appl. Therm. Eng.* **2018**, *129*, 290–305. [CrossRef]
69. Christen, E.J.; Blatchley, T.; Jacobson, M.; Ahmed, N.K.; Gong, Q. *Improving Range Robustness: Heat Pump Value for Plug-In Electric Vehicles*; SAE International: Warrendale, PA, USA, 2017. [CrossRef]
70. McIntosh, J. Do People Who Buy Their First Electric Vehicle Buy a Second One After? 2021. Available online: https://driving.ca/auto-news/news/do-people-who-buy-their-first-electric-vehicle-buy-a-second-one-after (accessed on 1 June 2022).
71. Park, K.-J.; Hwang, J.-Y.; Ryu, H.-H.; Maglia, F.; Kim, S.-J.; Lamp, P.; Yoon, C.S.; Sun, Y.-K. Degradation Mechanism of Ni-Enriched NCA Cathode for Lithium Batteries: Are Microcracks Really Critical? *ACS Energy Lett.* **2019**, *4*, 1394–1400. [CrossRef]
72. Liu, L.; Li, M.; Chu, L.; Jiang, B.; Lin, R.; Zhu, X.; Cao, G. Layered ternary metal oxides: Performance degradation mechanisms as cathodes, and design strategies for high-performance batteries. *Prog. Mater. Sci.* **2020**, *111*, 100655. [CrossRef]
73. Andre, D.; Hain, H.; Lamp, P.; Maglia, F.; Stiaszny, B. Future high-energy density anode materials from an automotive application perspective. *J. Mater. Chem. A* **2017**, *5*, 17174–17198. [CrossRef]
74. Lane, B.W. From early adopters to early quitters. *Nat. Energy* **2021**, *6*, 458–459. [CrossRef]